processes

MDPI

*Review*

# Review of Motion Simulation of Particulate Matter in the Respiratory System and Further CFD Simulations on COVID-19

**Di Zhu *, Ezanee Gires, Huizhen Dong, Aolin Chen and Kamarul Arifin Ahmad ***

Faculty of Engineering, University Putra Malaysia, Selangor 43400, Malaysia
* Correspondence: gs59509@student.upm.edu.my (D.Z.); aekamarul@upm.edu.my (K.A.A.)

**Abstract:** Respirable particulate matter (RSP) is currently very harmful to the human body, potentially causing pulmonary silicosis, allergic rhinitis, acute bronchitis, and pulmonary heart disease. Therefore, the study of the deposition pattern of RSP in the human respiratory system is key in the prevention, treatment, and research of related diseases, whereby the main methods are computer simulation, in vitro solid models, and theoretical analysis. This paper summarizes and analyzes past deposition of RSP in the respiratory tract and also describes them in specific case studies such as COPD and COVID-19 patients, based on the review of the evidence, direction, and focus of future research focusing on simulation, experimentation, and related applications of RSP deposition in the respiratory tract.

**Keywords:** computational fluid dynamics (CFD); deposition of respirable particulates; respiratory system; COVID-19; transport of respirable particulates



**Citation:** Zhu, D.; Gires, E.; Dong, H.; Chen, A.; Ahmad, K.A. Review of Motion Simulation of Particulate Matter in the Respiratory System and Further CFD Simulations on COVID-19. *Processes* **2023**, *11*, 1281. https://doi.org/10.3390/pr11041281

Academic Editor: Haiping Zhu

Received: 14 March 2023
Revised: 11 April 2023
Accepted: 13 April 2023
Published: 20 April 2023



## 1. Introduction

In 2019, a new class of coronavirus-linked pneumonia was discovered by experts in Wuhan, the capital city of Hubei Province, China. The World Health Organization named it the novel coronavirus disease 2019, or COVID-19 [1], caused by the severe acute respiratory syndrome coronavirus (SARS-CoV-2) [2]. The pandemic caused by the novel virus triggered a serious blow to the global economy, as well as healthcare systems. At the beginning of the pandemic, the virus spread rapidly across the planet, except for four countries, which included North Korea and Tuvalu [3].

According to the Center for Systems Engineering and Science (CSSE) at Johns Hopkins University, as of 4 May 2022, the global cumulative number of confirmed new coronary pneumonia cases exceeded 51,478,766 and continues to climb [4,5]. While 6,240,555 deaths were reported, the actual number is expected to be far greater due to the high proportion of asymptomatic infections and limited detection capacity [6].

Highly infectious and spreading rapidly, the new coronavirus [7,8] is transmitted in various ways, with the most important ones being direct, aerosol, and contact transmission. Direct transmission occurs mainly by coughing or face-to-face conversation whereby droplets are sprayed and directly inhaled by others [9]. Therefore, masks were mandated in public and crowded places to minimize transmission.

Aerosol transmission is the formation of aerosols from droplets containing the Neo-Coronavirus mixed with the air, which are inhaled and continue to infect the respiratory system. Contact transmission occurs when droplets containing the virus adhere to the surface of an object. As the NeoCoronavirus particles are extremely stable and insidious, they can survive for different periods of time on different surfaces, sometimes reaching several days [10,11].

Some infected patients can be completely cured, but for others, clinical symptoms will persist. When patients have persistent symptoms for 4–12 weeks, it is referred to as long COVID, a term coined in the UK [12–14]. Symptoms also vary by age, gender, geography,

and physical fitness; to date, there are approximately 200 different clinical symptoms (See Tables 1 and 2) [15,16]. Some patients recovering from COVID-19 also develop sequelae such as abnormal insulin tolerance and β-cell function, thyroid function, urinary system, and skin, as well ashair loss and conjunctivitis [17–23]. In-depth understanding of the various properties of COVID-19 is an important research direction for humans at present.

**Table 1.** Sleep problems before and after the patient's illness [16].

| Sleep Problems Before and After the Patient's Illness | | |
|---|---|---|
| **Sleep Symptom** | **Experienced During Illness (of All Participants)** | **Had Symptom before Illness** |
| Insomnia | 60% (67.1 to 70.1%) | 21% |
| Night Sweats | 41% (39.2 to 42.4%) | 16% |
| Awakened Feeling | 36% (34.5 to 37.6%) | n/a |
| Unable to Breathe | | |
| Restless Legs | 18% (16.6 to 19%) | 14% |
| Sleep Apnea | 10% (9.5 to 12.8%) | 34% |
| Vivid Dreams | 33% (31.5 to 34.5%) | 23% |
| Nightmares | 26% (24.3 to 27.1%) | 20% |
| Lucid dreams | 15% (14.2 to 16.6%) | 34% |

**Table 2.** Test results for latent disease [16].

| Test Results for Latent Disease | | | | |
|---|---|---|---|---|
| **Virus** | **Positive** | **Positive (Past)** | **Negative** | **Total Tested** |
| Epstein-Barr (EBV) | 40 | 309 | 231 | 580 |
| Lyme Disease | 7 | 34 | 366 | 407 |
| Cytomegalovirus (CMV) | 4 | 85 | 204 | 293 |

*Respiratory System*

The respiratory system, as a major physiological system, is the most severely compromised in COVID-19 patients [24]. As Figure 1 shows, the respiratory system mostly consists of the upper and lower respiratory tracts and the lungs [25]. The upper respiratory tract mainly includes the nasal cavity, oral cavity, pharynx, and larynx. The lower respiratory tract mainly includes the trachea, main airways, and airways within the lungs. The most important component of the lungs is the alveoli, which are used as sites of gas exchange [26].

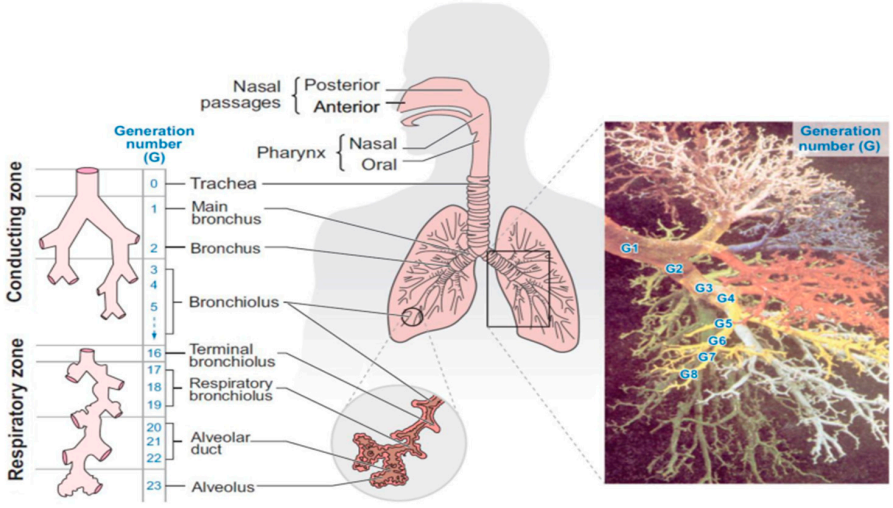


**Figure 1.** Exploded diagram of the human respiratory system [25].

## 2. Effects of Particulate Matter on the Human Body

Harmful particulate matter enters the body through the human respiratory system and may induce lung cancer, pneumoconiosis, and many other respiratory diseases [27], while most of the effects are irreversible, such as pulmonary heart disease and severe asthma [28–30]. It is generally accepted that the location of particle deposition is dependent on the particle diameter or size. Figure 2 shows the size of a human respirable particulate matter (RSP). In the 1930s, on particles with a particle size of 2.5 microns (PM2.5), the American Cancer Society (ACS) conducted cohort research of long-term health responses to living with particulate matter [31], and found that for every 10 μm increase in PM2.5 concentration, the risk of all-cause mortality, cardiopulmonary disease mortality, and lung cancer mortality increased by 6.2%, 9.3%, and 13.5%, respectively. The impact of inhalable particulate matter on the degree of health, and respiratory diseases and cardiovascular system diseases has the most significant relationship with the exposure level of particulate matter in the atmosphere. Long-term production and living in the environment of particulate matter will not only affect health, but also seriously affects lifespan. Different concentrations have different effects on human beings. The higher the concentration, the greater the impact on human lifespan [32,33]. The increase in the concentration in the atmosphere causes the incidence of cold and cough in adult men and women to increase, and the probability of triggering asthma in children will be very high. At the same time, the content of PM2.5 and PM10 per cubic meter in the atmosphere is positively correlated with children's respiratory inflammation, mild cardiovascular and cerebrovascular diseases, and children's induced asthma. Particles can also stimulate the sympathetic nerves in the lungs to produce secondary nerve sympathetic reflexes. Under an environment of PM2.5 and PM10 concentrations, the secondary nerve sympathetic reflexes of the human body are also different, which will change the autonomic nerve reflexes and other mechanisms to varying degrees and trigger the heart rate including arrhythmias and premature heart beats, and other cardiovascular and cerebrovascular diseases [34]. Living in a high-concentration environment for a long time will not only affect health, but also the normal development of the fetus, which will lead to congenital deformities in newborns, and even reduce human fertility and lead to an increase in the infertility rate [35]. The risk of harm of particulate matter to the human body increases at high concentrations. In a year when the concentration of particulate matter reaches its peak, the incidence of acute respiratory diseases and acute cardiovascular and cerebrovascular diseases will increase significantly. This short-term health effect is called the short-term effect. Anderson et al. [31] showed in the study of short-term exposure to PM10 that when the concentration of PM10 increases by 10 $\mu g/m^3$, the mortality rate caused by related diseases will increase by 0.6%. In deaths caused by cardiovascular diseases, a 0.9% increase in the mortality rate is associated with a 1.3% increase in the mortality rate due to respiratory diseases. Long-term exposure to an environment with a low concentration of particulate matter can also cause a variety of chronic respiratory diseases, and cardiovascular and cerebrovascular diseases. This kind of damage to the human body is called long-term effects. The American Cancer Society (ACS) analyzed the human body exposed to a low concentration environment for a long time [34] and concluded that when the concentration is PM2, the death rate from lung cancer will increase by 9.3%, and the death rate from lung cancer will increase by 13.5%. When the content of PM2.5 per cubic meter in the air increases, the chances of myocardial infarction and atrial premature beats in patients with coronary heart disease will greatly increase. The higher the concentration of PM2.5, when the particles enter the human blood circulation system, the more the viscosity of the blood will increase, and the content of some albumin in the blood will also increase, which will lead to an increase in the formation rate of thrombus. Samet et al. [36] studied the relationship between PM10 and cardiovascular diseases of local residents in 20 cities across the United States. The study showed that when the concentration of PM10 improved by 10 $\mu g/m^3$, the fatality rate caused by cardiovascular diseases would increase by 0.68%. Popet et al. [37] found that the concentration of PM2.5 has a strong relationship with acute unstable angina pectoris

and acute myocardial infarction. For every 10 μg/m$^3$ increase of the content of PM2.5 per cubic meter in the air, the incidence of acute unstable angina pectoris and acute myocardial infarction wouldincrease by 4.5%, and it would have a greater impact on the incidence of coronary artery disease (angina, heart failure, arrhythmia, etc.). In spring–summer and autumn–winter, when the content of PM2.5 per cubic meter in the air increases by 10 μg/m$^3$, the hospitalization rate of COPD patients will increase by 6.87% and 1.72%, respectively [38]. A study on the incidence of asthma patients showed that [39] the acute incidence of asthma patients is positively correlated with the content of PM2.5 per cubic meter in the air. When the concentration of PM2.5 increases by 10 μg/m$^3$, the total number of hospital visits increases by 0.67%. Visits to the emergency department increased by 0.65%, and visits to emergency departments increased by 0.49%. The American Cancer Society Survey Ffollowed over 1 million adults living in the U.S. between 1982 and 2008 and found that for every 10 μg/m$^3$ increase in PM2.5 concentration, the mortality rate from lung cancer would increase by 15% to 27% [40]. The amount of particulate matter per cubic meter of air in the atmosphere has a great impact on humanss. Whether it is PM2.5 or PM10, particulate matter of different particle sizes poses different hazards to the cardiovascular, cerebrovascular and respiratory systems of the human body at different concentrations. Therefore, it is very important to reduce air pollution and improve air quality.

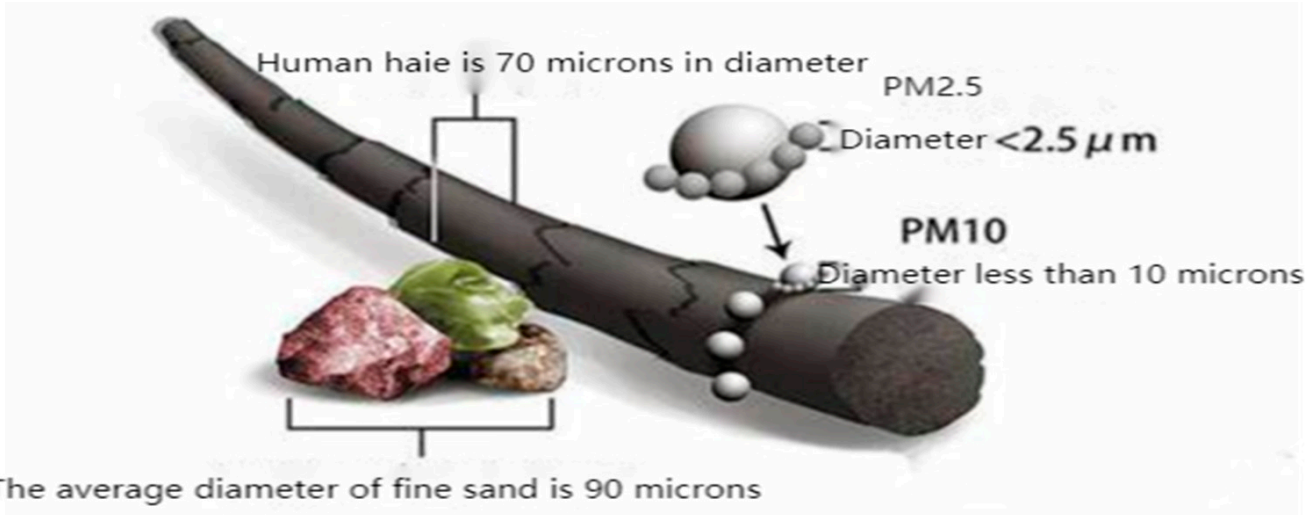


**Figure 2.** Size of human respirable particulate matter.

The human health condition tests from six major cities in the United States demonstrated that for every 10% increase the amount of particulate matter per cubic meter of air in the human space, the rate of human respiratory disease increased by 17.8% [41]. The production of life produces large amounts of solid particles, which are deposited in the human respiratory system and lead to a large number of diseases [42,43]. Various studies on the effects of particulate matter on the respiratory system demonstrated that air particulate matter concentration significantly impacts the respiratory system [44]. For instance, the computerized tomography (CT) imaging of the chest of COVID-19 patients revealed single or multiple ground glass shadows, crazy pavement disease, patchy glassy shadows with partial solidity, and solid lung lesions [45–47], all of which affect regular breathing. The deposition of particulate matter also varies in environments with extreme humidity [48–50]. For example, high and low temperatures affect the deposition and transport of particulate matter in the respiratory system [51].

A large number of data show that the degree of harm caused by particulate matter depends on the deposition site and amount of particulate matter deposited [52].

## 3. Deposition of Respirable Particles in the Upper Respiratory Tract

The upper respiratory tract is the first contact point and passage of inhaled particles. Of this section, the nasopharyngeal part is the first site of particle deposition. It is also made up of complex structures, including the inner wall with mucous membranes and fine cilia, that greatly influence the entry of respirable particles into the trachea and lungs [53].

Sun et al. [54] performed multilayer spiral CT coronal scans of the nasal cavity in 40 healthy subjects and then imported the data into the Ansys 12.0 software for surface 3D reconstruction. The nasal airflow field was analyzed by solving the N-S equation, and it was concluded that the nasal airflow in the nasal cavity was mainly through the middle and lower part of the common nasal tract. The analysis also found that the airflow was mainly laminar in the nasal cavity, free diffusion was mainly in the maxillary sinus cavity, and the air velocity in the maxillary sinus cavity was almost 0 m/s.

Cui et al. [55] used the neuron reconstruction algorithm (NeuRA) to construct a surface mesh from CT scanned nasal cavity data. The Ansys Integrated Computer Engineering and Manufacturing code for computational fluid dynamics (ICEM-CFD 11.0) was used to generate the volume network, and unidirectional and bidirectional coupling was used for different particle volume fractions. The N-S equation was again used to describe the airfield flow. It was concluded that particle deposition was related to particle size, particle release location, suction airflow rate, and geometric properties. Moreover, the turbulent and reflux zones have a strong influence on particle transport.

Soo-Jin Jeong et al. [56] constructed a CFD model from raw data of CT images from obstructive sleep apnea (OSA) patients and used the k-εmodel of a low Reynolds number by solving the continuity and Reynolds mean N-S equations (Equation (1)) to deduce the most collapsed region in the pharynx. The most collapsed region in these OSA patients was the area with the lowest intraluminal pressure, while the palatopharynx, where the pneumatic force is greatest, is also the area of the pharynx most prone to deposition of particulate matter. In another similar study, Wang et al. [57] performed CT scans of the nasal region of patients with OSA before and after surgery and developed an anatomical model of the interplay between the upper respiratory tract and soft palate. Computational simulations of expiration and inspiration were performed using flow-solid coupling, and the feature of airflow such as flow velocity and displacement distribution of the soft palate were selected for comparison. Airway resistance was found to be significantly reduced after nose surgery, particularly in the palatopharyngeal region. The results also showed that the airflow distribution and soft palate motion throughout the upper airway improved after nasal surgery, and the deposition of particulate matter became significantly greater.

$$\begin{gathered} \frac{\partial u_i}{\partial x_i} = 0 \\ \rho u_i \frac{\partial u_j}{\partial x_i} = -\frac{\partial P}{\partial x_i} + \frac{\partial}{\partial x_i}\left[\mu\left(\frac{\partial u_i}{\partial x_j} + \frac{\partial u_j}{\partial x_i}\right) - \rho\overline{u_i' u_j'}\right] \end{gathered} \quad (1)$$

$X_i$ are the Cartesian coordinates (= $x$, $y$, $z$), and $\mu_i$ are the Cartesian velocity components.

Cisonni et al. [58] scanned the human nasal cavity and constructed a three-dimensional model with the objective of performing virtual maxillary sinus surgery. The movement of air between the nasal cavity and sinuses during upstream pharyngeal aspiration were quantified, and the patient experienced dramatic changes in ventilation and had a significantly greater deposition of inhaled fine particulate matter in the sinus region. Cheng et al. [59] used silicone material to replicate a 3D model of the upper respiratory tract based on the airway dimensions of volunteers. Simulation experiments were then performed for three breathing intensities (15 L/min, 30 L/min, and 60 L/min) and the deposition of nine different particulates sizes. The data show that respiratory intensity and particle size significantly affect the deposition of particles, and the deposition rate of particles is positively correlated with the flow rate and particle size. When the particle size is lower than 20 µm and flow rate is more than 60 L/min, the particle deposition efficiency reaches more than 90%.

Grgic et al. [60] used CT, magnetic resonance imaging (MRI), and direct observation of breathing of organisms using simple geometry fabrication to establish an ideal human oral airway model. Additionally, γ-scintillation scanning and weighing methods were utilized to analyze the effects of the size of the particulates, air respiratory intensity, and Reynolds number on the results of particulates deposition in the mouth airway. Through the deposition simulation of particulates with a particle size of 3.5 μm and 6 μm at a flow rate of 0.5 L/s and 15 L/s, respectively, it was demonstrated that respiratory intensity, particle size, and inertia affect particulates deposition, while the pharynx and larynx are the main deposition sites of aerosol particles. Martonen et al. [61] further established a two-dimensional model of the human larynx and upper part of the tracheal, and used the N-S equation for flow-field analysis. Using the human throat at three different gas velocities of 15 L/min, 30 L/min, and 60 L/min, and according to the Reynolds value of the designated position inside the human body system (Table 3), the study concluded that the laryngeal flow field is complex, generating local vortices and jets at the acoustic portal, which significantly affect the distant flow field and can impact the deposition of particulate matter entrained in the air in the human larynx.

**Table 3.** Reynolds number at a given location inside the human body system [61].

| | **Inspiration Flow Rate (L/min)** | | |
|---|---|---|---|
| Lacation | 15 | 30 | 60 |
| Venteicular folds | 1600 | 3200 | 6400 |
| Vocal folds | 1970 | 3100 | 4740 |
| Trachea | 1160 | 2320 | 4640 |
| Main bronchi | 855 | 1710 | 3420 |

Xi et al. [62] utilized a coupled computational fluid dynamics (CFD) method for system parameter studies and steady-state flow simulation to replicate in vitro experiments by CT scans of the adult mouth, nose and throat. The data found differences in the amount of respirable particulate matter deposited and the deposition rate in the upper respiratory tract between dynamic and static vocal tracts. The data also revealed that the larger the cross-sectional area of thevocal tract region of the human larynx, the more pronounced the deposition of particulate matter. The complexity of the model has a great influence on the computer simulations' results. The difference between the USP IP and real model reaches 55%, and when the particle size of the experimental surface is 6–12 μm, the particle deposition rate and particle geometry correlation is the largest, reaching 45%. Grgic [63] further developed a new procedure to measure the factors affecting deposition by measuring the deposition of dioctylphthalate (DOP) particles with a particle size of 5 μm at a moving speed of 30 L/min. The results demonstrated that the deposition of particles in the mouth increases significantly during an unsteady flow. However, when the moving speed reached 40 L/min and above, the deposition in the oral cavity did not significantly change.

Kim et al. [64]. conducted a simulation study of aerosol particle deposition by two models, the inside-out branching and the 90° face branching models. The research indicates that the deposition efficiency of aerosols in the upper airway at a fixed Reynolds number became larger as the Stokes number (SKS) became larger. However, when the value of SKS was lower than 0.002, the deposition results did not significantly differ for either model. Zhou et al. [65] simplified the human upper respiratory system by using the nose, throat, oral and bronchi of an adult cadaver as a solid model, while a simple upper respiratory tract model was bent for simulation experiments. Particle sizes from 0.93 to 30 μm were injected into the two models at different flow rates to derive the deposition equation. The equation determined the deposition rate of the lung dose was in general agreement with the results derived from the theoretical model.

Li et al. [66]. used acrylonitrile butadiene styrene (ABS) material to create a 3D model of the human respiratory system and used this model to study the deposition of toxic respirable particles to explore selected respiratory disease treatments. The deposition conditions at two particle sizes of 0.3 and 6.5 μm and two different flow rates of 30 and 60 L/min were simulated. Particle size had little effect while moving speed had a greater effect on the deposition rate; the error between the two was not more than 2.5%. Phuong et al. [67] used particle image velocimetry (PIV) to measure the trajectories and motion patterns of particles at 7.5, 15 and 30 L/min in three different flow velocities, and CFD was used to simulate four types of turbulence for the experimental model. A comparison of the results obtained from both approaches revealed that both approaches were in high agreement, The agreement is about 87.6%. Jia et al. [68] studied the deposition of particles of different sizes. Kiasadegh et al. [69,70] studied the deposition of respirable particles through form changes in the human upper respiratory system. A simple oral cavity model was used by Chen et al. [71] for the effect of mutual heat exchange between the air and oral mucus on the deposition of particulate matter; the results indicated that at a moving speed of 15 L/min, the interaction between the hot gas flow and mucus layer had an effect on particulate matter deposition in the human body, and the interaction between the two could reduce the deposition rate of particles by 10%.

Based on the above review, the nasopharyngeal region of the upper respiratory tract is the first checkpoint for particulate matter to enter the respiration tract, while structural and human breathing patterns directly affect the distribution of particulate matter deposition in this region, as well as their entry into the airway and deep lungs.

## 4. Deposition of Respirable Particulate Matter in the Bronchial Tubes

The bronchi are an important research target for PM deposition, with a specific focus on bronchial fraction. Taherian et al. [72] simulated the sinusoidal behavior of normal respiration and corresponding exit pressure by assigning appropriate boundary conditions, using a Lagrangian model for 2.5 and 10 μm respirable particles. The data demonstrated that the high vortex, secondary flow, and high wall shear stress regions are strongly associated with particle deposition, and that the deposition number of 2.5 μm sized particles was much lower than 10 μm particles; the difference between them is about 57.9%. Rhein et al. [73] found that the total deposition of the pressure constant, volume ramp, and rising ramp waveforms was similar to the fourth waveform, which is the pressure sinusoidal waveform, but the deposition rate of the sinusoidal waveform was approximately 50% lower than that of the other waveforms, and the pressure positive waveform can reduce the wall shear stress by 75%. This indicates that the breathing pattern affects the deposition of PM in human lungs.

Sracic et al. [74] simulated variedly sized (0.05, 0.1, 2.5 and 10 μm) particles utilizing the multipath particle dose (MPPD) computer modeling method and concluded that lung deposition of large PM (2.5 and 10 μm) particles slowly decreased during exercise. The RSP of small particle size, on the other hand, slowly increased during exercise. Islam et al. [75] obtained real human airway data through CT scanning and simulated the deposition and movement of diesel exhaust particulate matter (DEPM) using the Lagrangian particle tracking method. The quantitative data indicated that during rapid breathing, higher surface deposition concentrations was noted in the upper part of the trachea, while during slow breathing, lower depositions were concentrated in the upper trachea. During the transport of particles in the same tracheal part, the concentration was higher in the right bifurcation of the lung during rapid breathing and lower during slow breathing. The results of the deposition and transport of inhalable particulate matter caused by different breathing methods are different.

Rahimi-Gorji et al. [76] studied air moving and particle deposition under three different breathing speeds, namely light (15 L/min flow rate), normal (30 L/min flow rate), and heavy (60 L/min flow rate). The moving and deposition of the particles were evaluated by a CT figure of the human respiratory tract, puted into CATIA V5 software for modeling and

other operations, and also imported into the ABSYS FLUENT using the Lagrangian method. The highest deposition rate was obtained for particulate matter with diameters between 5 and 10 μm during normal breathing (30 L/min flow rate). The deposition rate was highest when the particles were 1 μm in diameter and during light breathing (15 L/min flow rate). The resultant surfaces were affected based on inertial collisions respiratory patterns of the RSP with different diameters.

Lintermann et al. [28] researched the deposition of aerosols in the human upper tracheobronchial airway by using a unidirectional coupled Euler-Lagrange method to investigate particle flow. Aerosol flow was also accompanied by particle solvers by simulation with the Lattice Point-Boltzmann method. Here, 0.32 of the heavier and larger particles were deposited into the deeper parts of the airway. Moreover, only 0.069 of particles with a size of 2.5–10 μm were deposited in the first six Bronchus. These areas included the primary bronchi, large lobe bronchi, and segmental bronchi, indicating that most of the respirable particles within the range of 2.5–10 μm were deposited in deeper sites and would have a greater impact on the body. In another study, Shen et al. [77] investigated the factors influencing the deposition of particulate matter in the human respiratory system by establishing a 3D numerical model of the respiratory tract in normal humans. The study was conducted by simulating the distribution pattern of airflow during inhalation and changing parameters such as particle diameter, density, and respiratory airflow rate through comparative analysis. It was concluded that the particles were mostly deposited in the airway where the geometry was complicated or airway direction was drastically changed. The airway deposition rate was affected by particle diameter, density, and respiratory airflow rate.

The studies above assumed that particulate matter was a regular spherical shape, which was also the assumed ideal existential state. Nevertheless, irregularly shaped particulate matter was also studied. For example, Dastan et al. [78] studied the deposition distribution of irregular respirable particulate matter in the four cases of flow rate of 2.5, 5, 7.5 and 10 L/min respirable particles in the nasal cavity by solving the Navier-Stokes and continuity equations, to evaluate the airflow field in the nasal cavity. The study concluded that the aspect ratio of non-spherical RSP is an important factor when studying deposition distribution patterns.

Additionally, Sturm et al. [79] simulated the moving and deposition of particles in individual structures of the trachea and bronchi tract by studying the inhalation of aerosols and RSP in people of different ages. The RSP were of different shapes and sizes, and a stochastic model of the bronchus tree with thorough research and analysis of deposition equations was used. The resulting amount of surface deposited mass was positively correlated with age, with a lower probability of reaching the alveoli in infant and pediatric lungs but mostly in adolescent and adult lungs. These studies suggest that the RSP's surface, size, shape, and other factors can significantly impact the deposition of particulate matter in the airways.

Zhang et al. [80] useda modified commercial finite-volume code approach to simulate the effect of the impact and settling on the transport and deposition of particulate matter, and concluded that impactors were medium-sized at flow rates of 15–30 L/min.The main influencing mechanism of the airway, and for the large-sized airway, the subsidence, plays a decisive role at the moving speed of 3.75 L/min. Nicolaou et al. [81] performed direct numerical simulations of an oropharyngeal model (Figure 3) and a bifurcated airway model to investigate the moving and deposition of PM in these two models. Here, simulation results were compared without the effect of gravity. It was discovered that the particles with a high Stokes number were mainly deposited in the mouth, larynx, trachea, and subbranch. This impact and deposition had a positive effect on the deposition of respirable particles, while the final deposition results varied for different shapes of the bifurcated model, when the exercise intensity is high, the deposition rate of large respirable particles in the upper half of the bronchi is about 2.3 times that of small particles.

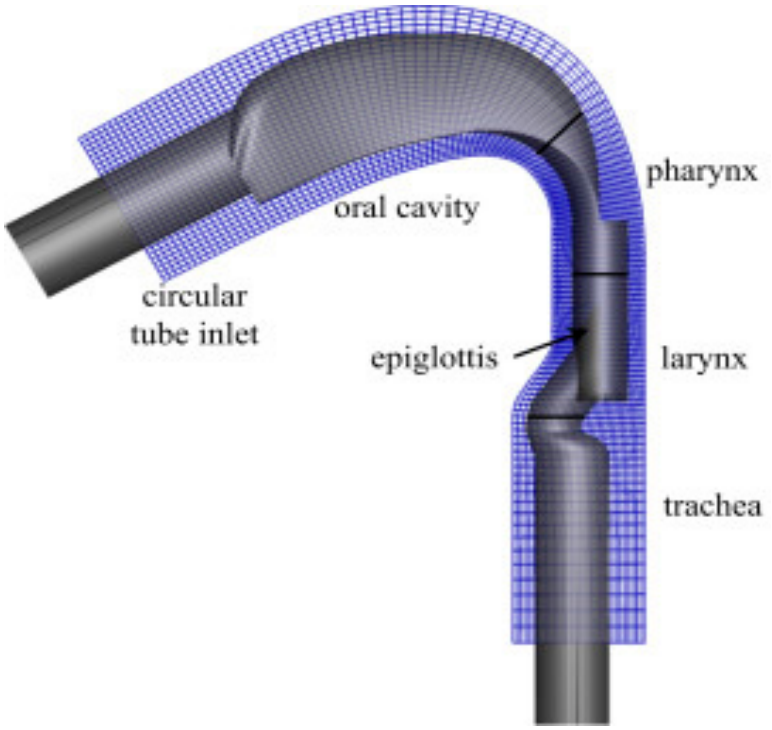


**Figure 3.** The idealized geometry and curvilinear grid adopted for the extrathoracic airways [81].

In another study, Lin et al. [82] simulated the trajectory of respirable fibers by solving a system of waste linear equations and the respiratory effects within the respiratory system. The results showed that the Brownian force is the most important factor influencing the movement and deposition of respirable fibers in the human trachea and bronchi. Feng et al. [83] used a newly proposed fluid particle motion model for the movement of e-cigarette aerosols at the G3-G6 trachea and compared the movement with the transport of traditional cigarettes. Data revealed that e-cigarettes had a greater impact on our trachea compared to cigarettes. Furthermore, Chen et al. [84] developed a new CFD-DEM program, which used analog computing in the deposition of PM in the human airways. Data revealed that the initial position of particles in the airways has a great influence on the final deposition position of respirable particles. CFD analysis of the deposition of respirable particles in the human airways also revealed the lack of uniformity at different motion intensities. Qihong Deng et al. [85]. used CFD to simulate the deposition of inhalable particle in the airway of the human body in polluted air, so as to study the impact of the human body in a polluted environment. The results showed that the deposition position of particles under different exercise intensities was inconsistent.

Modeling of the respiratory tract has gradually moved from modeling with anatomical data to modeling using computers. Due to the development of computer technology, scholars are now using CT or MR scans to model the respiratory tract. Rahimi-Gorji et al. [86] used computerized scanning technology (Figure 4) and CATIA modeling, to conduct research, and the conclusions drawn are closer to the real situation, with an error of no more than 12.1% from the real situation. Kabilan et al. [87] obtained geometry data based on CT scans of the respiratory tract. The scans modeled the entire tract, from the external section of the nose to the pulmonary airways, with a total of 272 exits in the human model. The study's data demonstrated that regional spore deposition patterns were sensitive to airway geometry and ventilation profiles, with approximately 6% of the 1 μm sized particles being deposited on the bronchi. Corresponding experiments using μ CT on rabbits further obtained airway geometry data for comparison with a solid radiological model and revealed 2878 exits.

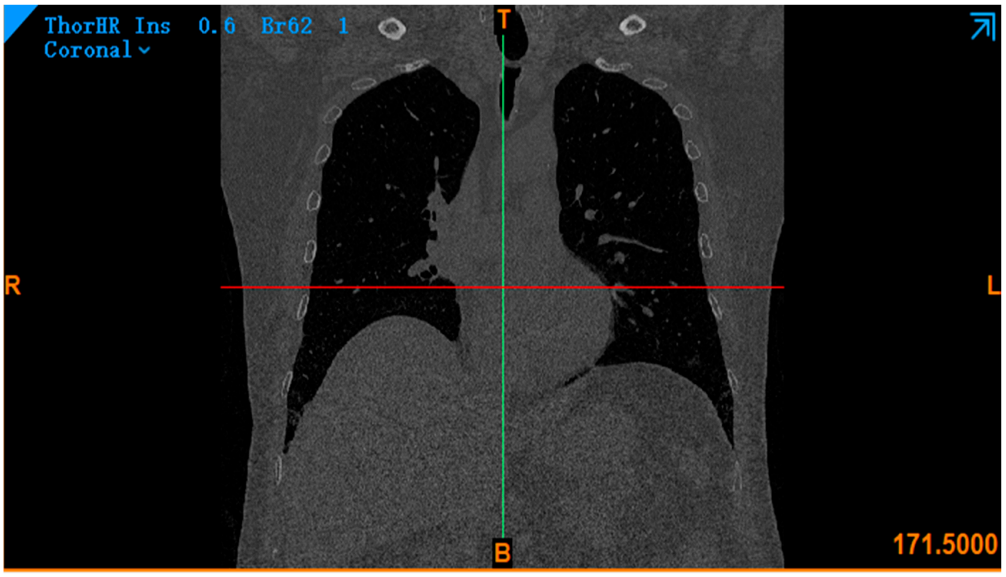


**Figure 4.** CT scan image of human lungs.

Although differences between the scans and reality are present, computer scans are rather accurate, advancing the field. Alternatively, Islam et al. [88] used the Euler-Lagrangian method to decipher the calculated continuous and discrete phases. The dispersion and deposition of DEPM nanoparticles in the developed anatomical model used a Lagrangian-based discrete phase model (DPM). Deposition distribution of the particulate matter was different between the left and right lungs of the human body, which could be due to the different structures of the human lungs.

Although previously, modeling data were obtained through dissection for simulation, which has its disadvantages, computer-based simulation also has its limitations. Computer-driven assumptions are based on an ideal scenario when the reality differs. Nevertheless, the challenges in obtaining an accurate distribution of particle deposition in the respiratory tract and radiopharmaceuticals can be misleading in the clinical setting. Therefore, the literature has comprehensively identified computer simulation as a method in the field of deposition of respirable particulates matter in the bronchial, which can be further developed by selecting suitable calculation conditions and methods for simulation.

Previous literature focusing on the bronchial part can be summarized as (1) deposition is relatively large when the diameter of respirable particles is 2.5–10 μm; (2) an increase in the deposition amount occurs when particles are less than 2.5 μm in diameter during light respiration, while when greater than 10 μm, minimum deposition is seen; (3) presently, all available and validated calculation conditions and methods are suitable to simulate deposition of respirable matter in the bronchial tubes, but further confirmation is needed for an optimal approach, and deposition of respirable particles in the bronchial is influenced by breathing patterns, such as flow of breathing.

## 5. Deposition of Respirable Particulate Matter in the Alveolar Region of the Lung

The pulmonary alveoli are composed of Class I respiratory fine bronchioles located distally within the lobules of the lung and the alveoli [89], acting as the basic functional unit of the lung. The pulmonary alveolar region is the most dominant region of respiratory function. Thus, the study of respirable particulate deposition in the pulmonary alveolar region is key for particulate-induced lung diseases, but also challenging. At present, the study of pulmonary alveoli is mainly divided into the single-alveolar and multi-alveolar models, both mainly studied utilizing computer simulation.

Due to the complexity of the alveolar region and the limitations of current computer technology, neither CT nor MR techniques can create a complete and realistic computer model of the alveolar region; therefore, simplified models are chosen for simulations when

studying the alveolar region. In a study, Żywczyk et al. [90] established a simulated single-cell model of the alveoli and used fluid-solid coupling simulation, as well as the Brownian dynamics algorithm to simulate the transport and deposition of aerosols.

As alveoli can have an effect on the deposition and transport of aerosols, both parameters indicate the alveoli's mechanical properties. Darquenne et al. [91] investigated the pattern of particle size deposition of respirable drugs in the lungs. A single-alveolar model was utilized since the whole-lung model was highly erroneous. The study found that when the particle size of respirable particles was less than 2 μm, the particles were mainly deposited in the alveolar region, and the deposition rate is as high as 89.6%. However, the local nature of the single-alveolar model makes it highly inconsistent with the deposition pattern of the real pulmonary alveolar model, suggesting the use of the multi-alveolar model.

Sznitman et al. [92] developed a three-dimensional alveolar motion model using regular respiratory motion and concluded that the alveolar flow pattern is independent of time. The study also determined that convective alveolar flow has an effect on the deposition of respirable particles at the alveoli. Sznitman et al. [93] also developed a multilevel alveolar duct model consisting of a simple alveolar duct and a space-filling asymmetric alveolar branching tree for simulating particles with particle sizes of 1 and 3 μm to study detailed particle trajectories and deposition efficiencies. This pipeline model also considers the alveolar flow structure to facilitate the study of surface particle trajectories and deposition rates that are closely related to gravity. These parameters indicate that highly variable deposits are produced for inhaled particles with different particle sizes. Haber [94] et al. further established a three-dimensional alveolar model for the relationship between alveolar wall motion and deposition and motion trajectories of respirable particles. Here, the motion of the alveolar wall was key to the deposition of respirable particulate matter; the deposition was heterogeneous within each alveolus.

Khajeh-Hosseini-Dalasm et al. [95] developed a new space-filling model of the alveolar region in order to study the correlation of aerosol deposition. The results demonstrated that the surface's alveoli had no effect on the total deposition of RSP after more than three generations of alveolar ducts, and that the orientation angle of gravity had no effect on the total deposition of particulate matter. Kolanjiyil et al. [96] modeled the entire pulmonary alveoli(Figure 5), with the alveolar portion approximated as a spherical attachment to a bifurcated airway duct. Analysis of the location of the surface alveoli revealed that its location affected the flow and deposition rate of the particulate matter, with the proximal lung region being dominated by the circulating flow.

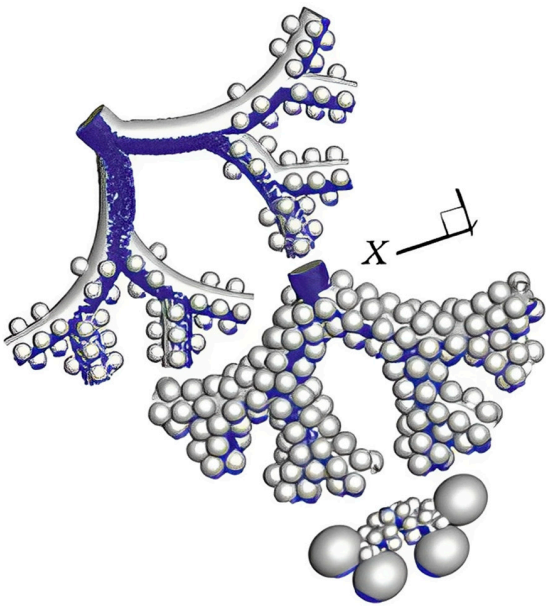


**Figure 5.** Simple human alveolar simulation [96].

More recently, the alveoli were studied based on the use of simplified alveolar models, which cannot completely simulate the real lung due to the huge number and variety of alveoli morphology in the alveolar region. Johannes [97] studied morphological changes to the alveoli by using three-dimensional visualization of the alveolar's capillary network obtained through high-resolution synchrotron X-ray tomography. This method allows a more complete simulation of the alveolar model in rats (Figure 6), but has not been applied to humans due to its biological component. Moraes et al. [98] further investigated the biological role of simulated organs, development of microbial engineering, and construction of human living organ tissues. However, no major progress was found in the study due to technical difficulties. Nevertheless, with the advancement of technology, complete modeling of the human alveoli for the study of deposition patterns of respirable particles can be achieved.

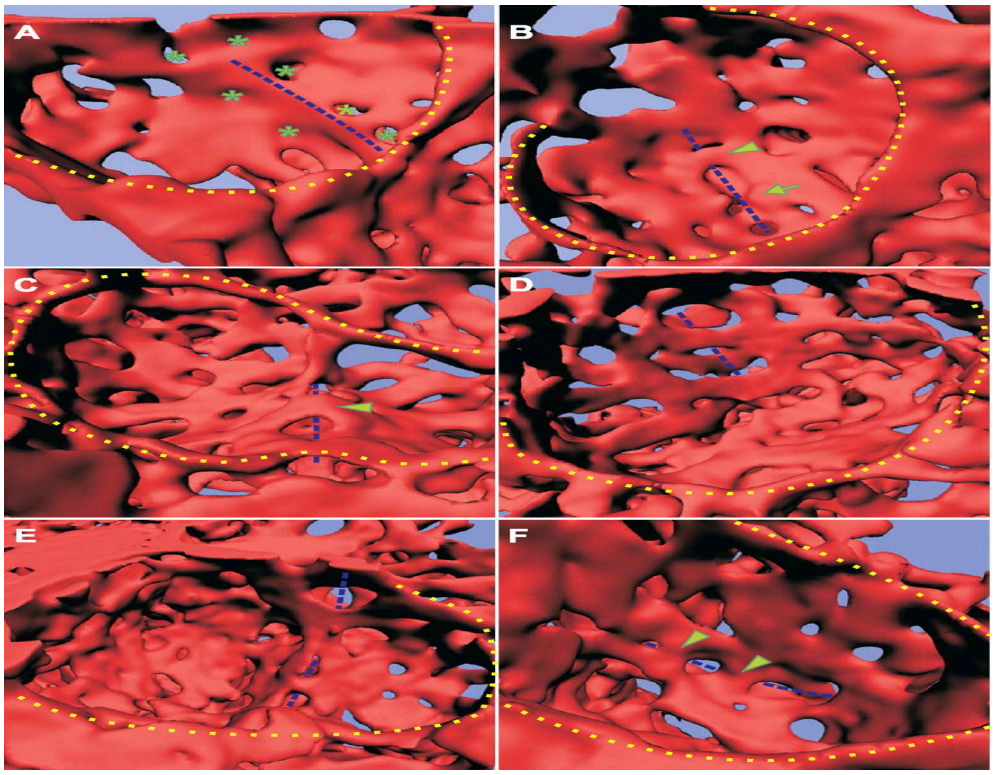


**Figure 6.** The 3D visualization model of the capillary network of the mouse lung, (**A**–**F**) are capillary views of alveoli at different angles. [97].

## 6. The Main Research Situation in the Past Five Years

Ching and Kajino [99], through the newly developed particle decomposition aerosol model, simulated the deposition of 5–20% inhalable soot particulate matter in the human respiratory tract, and proved the aerosol mixing index has a great effect on the final deposition efficiency F (Equation (2)).

$$F = \frac{\sum_{i=1}^{N} e_i(D_i, k_i) m_{soot,i}}{\sum_{i=1}^{N} m_{soot,i}} \quad (2)$$

where $e_i$ ($D_i$, $k_i$) is the deposition efficiency of particle $i$ with diameter $D_i$ and hygroscopicity $k_i$ and $m_{\mathrm{soot},i}$, is the mass concentration of soot contained in particle $i$.

Chantal et al. [100] studied the factors affecting the deposition rate of particles of different particulate matter sizes in the respiratory tract. The particles in the respiratory tract are not only affected by inertia, gravity and Brownian motion, but also by the interaction between turbulence. When the particulate matter size is ≥5 μm, most of the particles are deposited in the upper respiratory tract; when the particulate matter size is 2–5 μm, the

particles are deposited in the lower respiratory tract; when the particulate matter size is ≤2 μm, the particles are deposited in the alveoli. Li et al. [101], by using the finite difference way to solve the equation, studied the deposition of particles from different sources in the respiratory system. The study found that soil particulate matter has a lower density and a larger particle size, and is deposited in the upper part of the lungs. Particulate matter is deposited in the lower half of the lungs due to its higher density and smaller particle size.

Manojkumar et al. [102], using the multiple path particle dosimetry (MPPD) model to study the sedimentation and deposition of PM2.5, PM10 and PM1.0 inhalable particles of three different particle sizes in the trachea; of which about 45% of PM2.5 and PM1 particles were deposited in the lungs; found the PM2.5 sedimentation rate wass the highest, and the upper, middle, and lower parts are lobular sedimentation, accounting for 66.4%, 6.4%, and 27.2%, respectively. For the MDDP model, Manojkumar [103] also conducted a study on the influence of age and seasonal differences on the deposition rate. Using the MDDP model, the inhalable particulate matter of residents of different age groups in a certain area of India in different seasons was estimated. For deposition in the respiratory system, the research result shows that the total deposition rate of PM10 is the highest, and its deposition rate is significantly higher than that of PM2.5 in different age groups and different seasons, and the deposition rate of particles in summer is significantly higher. In other seasons, the accumulation rate of particles increased with age.

Khan [104] also used the MDDP model to analyze the respiration of PM1, PM2.5, and PM10 particles of three kinds of particle sizes in different age groups (3 months to 21 years old) in different seasons of monsoon, winter, and summer. The deposition conditions in the system have been simulated, and the research results show that the total deposition rate of particulate matter in winter is about 47%, which is significantly higher than the deposition rate of 45% in monsoon and summer. The deposition conditions are shownin Figure 7. The deposition rates of PM10, PM2.5 and PM1 in the respiratory tract are about 90%, 65% and 45%, respectively, that is, the deposition rate of PM10 in winter is the highest among all cases.

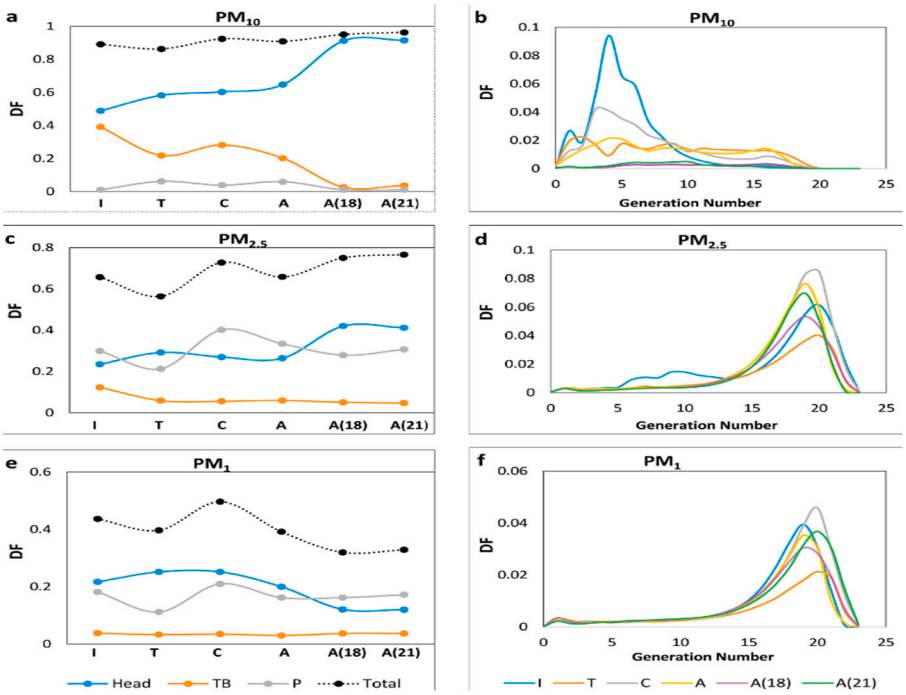


**Figure 7.** Total and regional DF (**a**,**c**,**e**) and DF as a function of the generation number (**b**,**d**,**f**) of PM10, PM2.5 and PM1 in different age groups. DF = deposition fraction; I = Infant; T = Toddler; C = Children; A = Adolescent; A (18) = Adult of 18 years; A (21) = Adult of 21 years.

For research on different age groups, Miao Liu et al. [105] conducted a special simulation study on children. This study mainly focused on whether children's blood pressure (BP) is related to the deposition rate of PM2.5 in the respiratory system. A total of 253 children in two cities in southern China were followed up and tested, and the MPPD model was also used for simulation to estimate the thoracic/head region (ET), trachea and bronchi (TB) and alveoli (AR). Regarding the deposition efficiency (DF) of particulate matter, through the relevant data (Table 4), it is concluded that the deposition of PM2.5 in children is closely related to children's blood pressure and interacts, and the deposition is related to children's prehypertension. Prevalence is also somewhat relevant.

**Table 4.** Associations of the tertile of human PM2.5 and its respiratory tract depositions with blood pressure and risk for prehypertension and hypertension at lag 2 day.

| | **SBP** | **DBP** | **MAP** | **Prehypertensi** | | **Hypertension** | |
|---|---|---|---|---|---|---|---|
| Exposure level | % Change (95% CI) | % Change (95% CI) | % Change (95% CI) | Case/Total | Odds ratio (95% CI) | Case/Total | Odds ratio (95% CI) |
| PM2.5 | | | | | | | |
| T1 (1.14–26.62 μm/m$^3$) | Ref. | Ref. | Ref. | 21/263 | Ref. | 30/263 | Ref. |
| T2 (26.73–49.26 μg/m$^3$) | 1.47 (−0.07, 3.02) | 2.00 (−0.22, 4.22) | 1.75 (0.05, 3.45) | 29/266 | 1.37 (0.75, 2.52) | 45/266 | 1.28 (0.76, 2.15) |
| T3 (49.41–341.60 μg/m$^3$) | 3.62 (1.84, 5.40) | 5.14 (2.55, 7.72) | 4.44 (2.47, 6.42) | 36/265 | 2.25 (1.13, 4.47) | 77/265 | 2.03 (1.17, 3.53) |
| P-trend | ≤0.001 | ≤0.001 | ≤0.001 | | 0.023 | | 0.013 |
| ET | | | | | | | |
| TI (2.82–68.26 μg) | Ref. | Ref. | Ref. | 16/264 | Ref. | 20/264 | Ref. |
| T2 (68.41–154.55 μg) | 2.66 (1.04, 4.29) | 1.46 (2.15, 6.76) | 3.64 (1.87, 5.41) | 27/265 | 2.34 (1.23, 4.44) | 37/265 | 2.02 (1, 4.09) |
| T3 (154.89–1644.8 μg) | 4.85 (2.91, 6.78) | 8.32 (5.54, 11.09) | 6.86 (4.74, 8.98) | 43/265 | 4.39 (2.03, 9.47) | 95/265 | 3.78 (1.77, 8.07) |
| P-trend | ≤0.001 | ≤0.001 | ≤0.001 | | ≤0.001 | | ≤0.001 |
| TB | | | | | | | |
| T1 (0.67–12.85 μg) | Ref. | Ref. | Ref. | 18/264 | Ref. | 25/264 | Ref. |
| T2 (12.96–25.14 μg) | 1.86 (0.33, 3.39) | 2.98 (0.79, 5.18) | 2.50 (0.82, 4.18) | 28/265 | 1.67 (0.87, 3.22) | 44/265 | 1.63 (0.90, 2.94) |
| T3 (25.15–190.61 μg) | 4.49 (2.74, 6.24) | 5.99 (3.44, 8.54) | 5.35 (3.41, 7.30) | 40/265 | 3.22 (1.56, 6.63) | 83/265 | 2.27 (1.24, 4.14) |
| P-trend | ≤0.001 | ≤0.001 | ≤0.001 | | ≤0.002 | | ≤0.006 |
| AR | | | | | | | |
| T1 (0.91–19.66 μg) | Ref. | Ref. | Ref. | 17/264 | Ref. | 20/264 | Ref. |
| T2 (18.7–39.34 μg) | 1.62 (0.04, 3.20) | 3.93 (1.68, 6.18) | 2.90 (1.18, 4.62) | 29/265 | 1.79 (0.93, 3.45) | 36/265 | 1.81 (0.95, 3.43) |
| T3 (39.53–319.54 μg) | 4.54 (2.64, 6.44) | 7.68 (4.95, 10.41) | 6.35 (4.27, 8.44) | 40/265 | 2.41 (1.15, 5.05) | 96/265 | 3.35 (1.72, 6.54) |
| P-trend | ≤0.001 | ≤0.001 | ≤0.001 | | ≤0.017 | | ≤0.001 |

Mean arterial pressure (MAP), Systolic blood pressure (SBP), Diastolic blood pressure (DBP).

Several studies have examined the question of whether outdoor sports and the performance of outdoor sports is related to the deposition of particulate matter. Zoladz et al. [106] conducted a simulation study on the running performance of marathon runners and the deposition of PM2.5 and PM10 in the human respiratory system. The research results show that when the breathing rate of ordinary marathon runners is 8 L/min, the deposition rate is 9 μg/h. When the breathing rate is 65 L/min, the deposition rate reaches 45 μg/h. For professional marathon runners, the deposition rate will be 22% higher than that of ordinary marathon runners. The analysis results show that there is a certain relationship between marathon performance and deposition rate, and there is an inverse correlation.

## 7. Deposition of Respirable Particulate Matter in Pathological Models

The general population is exposed to polluted air for prolonged durations due to unavoidable factors such as daily commute and occupation, leading to the development of respiratory diseases. As a consequence, pneumonia, bronchial obstruction and chronic obstructive pulmonary (also known as COPD) diseases have become common lung diseases [42,107], all of which affect the deposition pattern of particulate matter of the lungs. COPD is particularly associated with a high death rate [108,109]. Darquenne et al. [110] in their analysis of healthy individuals and patients with COPD found that the total deposition of aerosols did not significantly differ among any of these groups (Table 5). Additionally, total deposition increased with the diameter of the particulate matter and flow rate, but heterogeneity was greater in COPD patients. Ganguly et al. [111] experimentally simulated

the deposition of particulate matter in the lungs of COPD patients with varied success. Here, deposition, distribution and clearance of particulate matter in the lungs of COPD patients were greatly influenced by particle characteristics.

**Table 5.** The relevant anthropometric data of the subjects [110].

| Anthropometric Data | | | | | | | |
|---|---|---|---|---|---|---|---|
| **Health Status** | **Subject No.** | **Gender** | **Age** | **Height, m** | **Weight, kg** | **FEV Predicted** | **FEV/FVC** |
| H | 1 | M | 35 | 1.70 | 68 | 1.13 | 0.88 |
| H | 2 | M | 52 | 1.65 | 97 | 1.17 | 0.79 |
| H | 3 | M | 47 | 1.83 | 89 | 0.85 | 0.74 |
| H | 4 | M | 26 | 1.83 | 82 | 0.94 | 0.8 |
| H | 5 | M | 34 | 1.93 | 100 | 1.04 | 0.84 |
| H | 6 | M | 21 | 1.68 | 54 | 0.89 | 0.73 |
| H | 7 | M | 21 | 1.73 | 64 | 0.95 | 0.81 |
| C | 1 | M | 57 | 1.64 | 70 | 0.60 | 0.56 |
| C | 2 | M | 55 | 1.78 | 66 | 0.56 | 0.48 |
| C | 3 | M | 45 | 1.80 | 83 | 0.69 | 0.67 |
| C | 4 | M | 54 | 1.87 | 84 | 0.58 | 0.52 |
| C | 5 | M | 62 | 1.88 | 87 | 0.67 | 0.47 |
| C | 6 | M | 45 | 1.78 | 75 | 0.83 | 0.66 |

M: Male, F: Female, H: Healthy, C: COPD.

Wang et al. [112] elaborated on aerosol deposition, dissolution, absorption and clearance in diseased lungs, and found that varied lung lesions with varied degrees also greatly influenced aerosol deposition. Zhuang [113] discussed the moving and deposition patterns of respirable particulate matter in the respiratory tract of COPD patients utilizing mathematical physical models and numerical discussions. The effect of multiple factors such as obstruction rate and location, as well as work intensity, on the simulation results were analyzed. The results revealed that (1) respiratory tract deformation has an effect on the form of deposition, (2) the level of intensity of motion has a great effect on the symmetry of particulate matter deposition, and (3) the size of the particles has an effect on the deposition rate.

Tohidi et al. [114] simulated the deposition of micron-sized droplet particulate matter in the nasal cavity of two patients with nasal airway obstruction and showed that patients with nasal tract obstruction had significantly higher inertia than healthy individuals; the deposition rate increased by about 23.4%. The inertial mechanism was the main factor influencing the amount of deposition relative to the diffusion mechanism,. Deng et al. [88] simulated the airways of healthy and asthmatic patients with the gas-solid mix flow, utilizing three different flow rates. The research results revealed that the deposition rate of particulate matter was bigger in the asthma simulation, therefore concluding that asthmatic patients were more susceptible to PM2.5. Similar research was finished by Zhang et al. [115] for childhood asthma, where the airway of a 4-year-old with asthma was modeled in two dimensions; the airway diameter of the model was reduced by about 40% and 60% compared with normal children, and CFD was used to simulate the airway airflow as well as the deposition of particulate matter; the particle size of the particles was 1–10 μm. To investigate the influence of obstruction on particulate matter deposition in COPD patients, using the ideal COPD model (Figure 8), Luo et al. [116] used CFD to solve the three-dimensional incompressible N-S equation and showed that particle deposition had a significant effect (Figure 9) at the lower end of the obstructed airway.

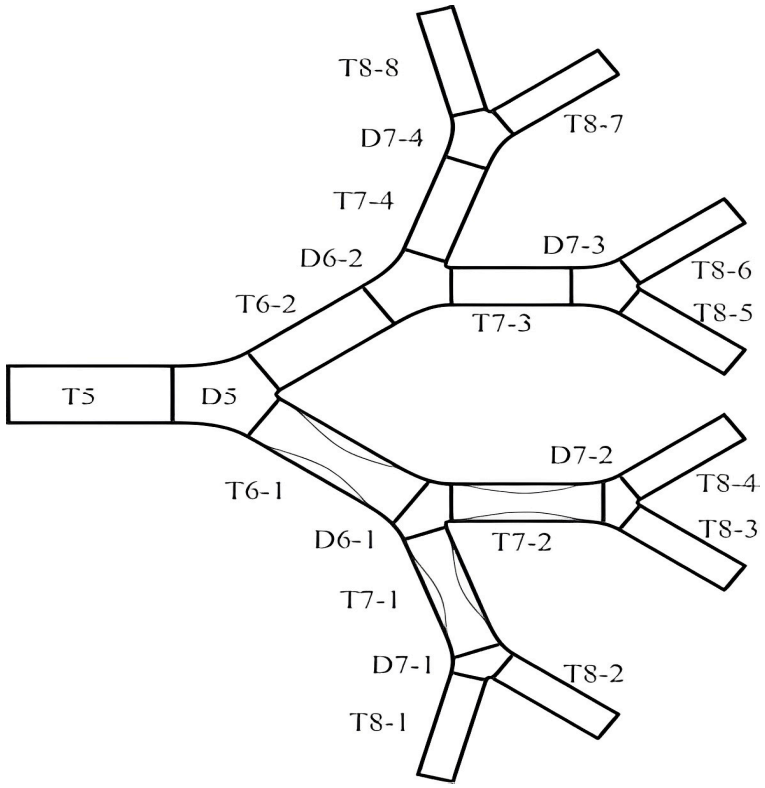


**Figure 8.** Airway diagram of a COPD patient (T6-1, T7-2, and T7-1 are the diseased airway) [116].

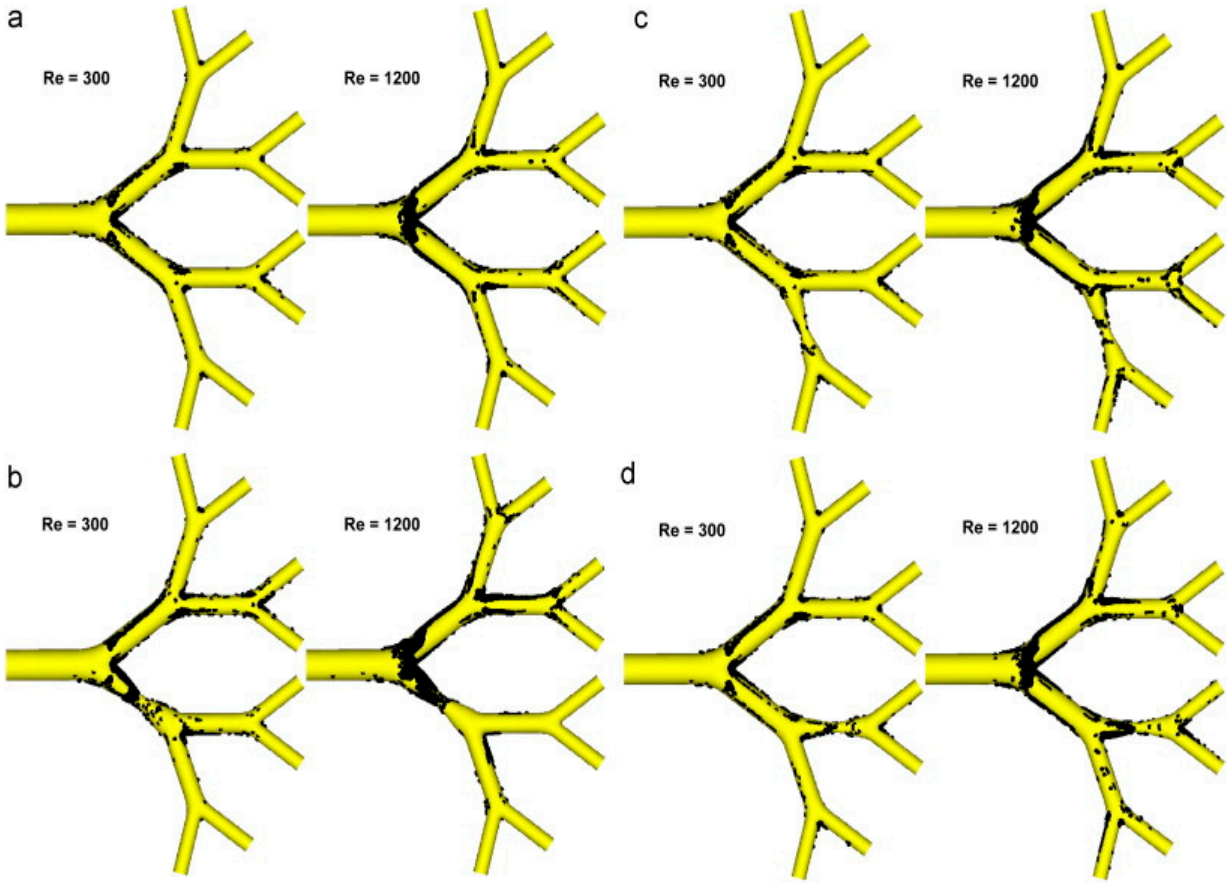


**Figure 9.** Particle deposition patterns of (**a**) Model 1, (**b**) Model 2, (**c**) Model 3, and (**d**) Model 4 [116].

## 8. Simulation of COVID-19 Models

In the present day, COVID-19 has become a major respiratory illness, warranting in-depth research. Prinz et al. [117] through a survey and study of 100,000 German residents (Tables 6 and 7), found that patients with COVID-19 who lived for a long time in an environment with large amounts of respirable particles in the air had a higher PM2.5; in the air with an increase of 1 $\mu g/m^3$, the incidence of COVID-19 patients will increase by 0.002%, and for each increased concentration of PM10 in the air by 1 $\mu g/m^3$, the incidence of COVID-19 patients will increase by 0.00053%. So in the air, there is a positive relational between the concentration of pollutants and the incidence of COVID-19. Bianconi et al. [118] investigated the mortality rate of COVID-19 patients and the air quality in various regions of Italy and showed that PM2.5 and PM10 in the air were responsible for increased mortality. Mehmood et al. [119] found that the level of PM2.5 in the air had a great influence on the incidence of COVID-19.

**Table 6.** COVID-19 cases per 100,000 inhabitants and Kriging-interpolated PM10 pollution [117].

| Variable | Basic Model | Standardized Coefficients | State Fixed Effects Model | Standardized Coefficients |
|---|---|---|---|---|
| Distance to Ischgl | −1.892 | −0.4349298 | −1.802 | −0.4141894 |
| Distance to nearest German hotspot | 1.782 | 0.1530381 | 1.955 | 0.1679186 |
| Nursing home places per 100 k inhabitants at 75 and older | 0.017 | 0.03517896 | 0.047 | 0.09850678 |
| Share of people >75 years | 3709.915 | 0.0668369 | 1551.69 | 0.02795485 |
| Population density | 0.275 | 0.2033308 | 0.167 | 0.1234201 |
| Commuter flow | −0.004 | −0.09751138 | −0.003 | −0.0743129 |
| Avg. PM10, 2002 to 2020 | 52.381 | 0.1689943 | 36.08 | 0.1164028 |
| Avg. Income 2002 to 2018 | 4.772 | 0.01166486 | 10.994 | 0.02687409 |
| East Germany | 544.945 | 0.2241532 | | |
| Border with Czech Republic | 1900.803 | 0.3644518 | 1422.722 | 0.2727866 |
| Constant | 1600.346 | | | |
| Fixed effects | NO | YES | | |
| Observations | 400 | | 400 | |
| Adj. R2 | 0.463 | | 0.145 | |
| F Statistic | 35.406 | | 10.166 | |

**Table 7.** COVID-19 cases per 100,000 inhabitants and Kriging-interpolated PM2.5 pollution [117].

| Variable | Basic Model | Standardized Coefficients | State Fixed Effects Model | Standardized Coefficients |
|---|---|---|---|---|
| Distance to Ischgl | −1.892 | −0.4349298 | −1.802 | −0.4141894 |
| Distance to nearest German hotspot | 1.782 | 0.1530381 | 1.955 | 0.1679186 |
| Nursing home places per 100 k inhabitants at 75 and older | 0.017 | 0.035117896 | 0.047 | 0.09850678 |
| Share of people >75 years | 3709.915 | 0.668369 | 1551.69 | 0.02795485 |
| Population density | 0.275 | 0.2033308 | 0.167 | 0.1234201 |
| Commuter flow | −0.004 | −0.09751138 | −0.003 | −0.0743129 |
| Avg. PM10, 2002 to 2020 | 52.381 | 0.1689943 | 36.08 | 0.1164028 |
| Avg. Income 2002 to 2018 | 4.772 | 0.01166486 | 10.994 | 0.02687409 |
| East Germany | 544.945 | 0.2241532 | | |
| Border with Czech Republic | 1900.803 | 0.3644518 | 1422.722 | 0.2727866 |
| Constant | 1600.346 | | | |
| Fixed effects | NO | YES | | |
| Observations | 400 | | 400 | |
| Adj. R2 | 0.463 | | 0.145 | |
| F Statistic | 35.406 | | 10.166 | |

A large body of literature also suggests that air pollution increases mortality in COVID-19 patients and sequelae in recovered patients [120–123]. Cruz et al. [124] studied the deposition of particulate matter during endurance exercise and the entry of the COVID-19 virus into the respiratory tract. A surface study of the virus revealed that COVID-19 enters the respiratory tract similarly to when the human body does endurance exercise. Workman et al. [125] studied the aerosol dispersion in the olfactory and respiratory epithelium of COVID-19 patients and discovered that olfactory dysfunction affected particle deposition in COVID-9 patients. Ongoing studies focusing on COVID-19 patients are proposing effective prevention and treatment options for the respiratory characteristics and physiological properties of COVID-19.

## 9. Future Key Research Directions and Contents

In summary, RSP has a great influence on the human respiratory system, and the flow and deposition pattern of particulate matter, slowly changing from universal to specific effects. The current research methods include theoretical analysis, computer simulation (CT and MR), and solid modeling mostly utilizing computer simulation. Future research is predicted to be on (1) the affection of various respiratory diseases on the deposition of particulate matter, (2) the influence of external factors such as temperature and humidity of the air during respiration, as breathing affects the humidifying and heating of air, (3) the validation of computer simulation experiments by comparing with the simulation of air and non-physical experiments, which would be better compared with physical animal experiments, 4) the biological characteristics of the human body, whereby computer simulation cannot completely simulate the human body, for example, the elasticity and viscosity of the bronchi, and the roughness inside the trachea. Therefore, these data are ignored during simulation, although they carry clinical significance for the in-depth study of the deposition of particulate matter.

## 10. Conclusions

This article introduces the impact of particles with different particle sizes on human health, and the impact on the human body at different concentrations. At the same time, it also introduces the moving and deposition of particulate matter in the upper respiratory tract, lower respiratory tract and pulmonary acinus of the human body, modeling the upper respiratory tracts and lower respiratory tracts in various ways, and then conducting CFD simulations, as well as research on the deposition of particles in the alveoli, and some typical ill-conditioned models are simulated. With the continuous advancement of technology, the continuous development of CT, MR and computer simulation technologies have an important role in the prevention, treatment and research of diseases caused by particulate matter and complications of some other diseases (such as COVID-19, COPD, lung cancer, etc.).

The next direction of work:

1. Since human respiration is a complex process, under normal circumstances, the respiration rate changes periodically with time, and the process of exhalation and inhalation will have a great influence on the deposition of particles. In future research, the effects of periodic changes in the respiratory rate in COVID-19 patients on particulate matter deposition should be considered.

2. Further research is needed on the deposition and transport of ultrafine particulate matter (PM $\leq$ 0.1) [126–128] and heavy metal particulate matter in the respiratory system of COVID-19 in humans.

3. Due to the underdevelopment of children's respiratory tract, children are more seriously affected than adults by the deposition of particles [129]. A study on the deposition of particles in children with congenital breathing diseases and infected with the COVID-19 virus, and research on the deposition of particulate matter in elderly persons with COVID-19 who suffer from geriatric diseases are future research topics. Another research area is the causes of harm to COVID-19 patients.

4. The incidence of certain respiratory diseases (such as asthma) at night is different from that during the day. It will be further discussed whether the deposition of particles in the respiratory system of COVID-19 patients is affected by night or day.

5. The production of inhaled COVID-19 targeted drugs and improvement of the targeting of drugs [130], and the precise delivery of drugs to lesions will be the main research direction of the World Medical Organization in the future. Inhalation therapy will be effective to treat COVID-19 and prevention will play an important role.

**Author Contributions:** D.Z.: Methodology, Formal analysis, Writing—original draft, Writing—review & editing. E.G., H.D., A.C. and K.A.A. Conceptualization, Resources, Writing—review & editing, Supervision. All authors have read and agreed to the published version of the manuscript.

**Funding:** This research received no external funding.

**Data Availability Statement:** Not applicable.

**Conflicts of Interest:** The authors declare no conflict of interest.

## References

1. WHO. Clinical Management of Severe Acute Respiratory Infection When Novel Coronavirus (COVID-19) Infection is Suspected: Interim Guidance [EB/OL]. Available online: https://apps.who.int/iris/handle/10665/330893 (accessed on 28 January 2020).
2. WHO. Naming the Coronavirus Disease (COVID-19) and the Virus that Causes it [EB/OL]. Available online: https://www.who.int/emerg-encies/diseases/novel-coronavirus-2019/technical-guidance (accessed on 25 January 2021).
3. Postma, M.J.; Chhatwal, J. COVID-19 health economics: Looking back and scoping the future. *Value Health* **2022**, *25*, 695–696. [CrossRef] [PubMed]
4. Johns Hopkins University. COVID-19 Dashboard by the Center for Systems Science and Engineering at Johns Hopkins University [EB/OL]. Available online: https://coronavirus.jhu.edu/map.html (accessed on 4 May 2022).
5. Chan, J.F.; Yuan, S.F.; Kok, K.; Hin, C.; Jin, Y.; Fanf, X.; Jiel, L.B.; Cyril, C.Y.Y.; Rosana, W.S.P.; HoiWah, T.M.; et al. A familial cluster of pneumonia associated with the 2019 novel coronavirus indicating person-to-person transmission: A study of a family cluster. *Lancet* **2020**, *395*, 514–523. [CrossRef] [PubMed]
6. Wu, S.L.; Mertens, A.N.; Crider, Y.S.; Nguyen, A.; Pokpongkiat, N.N.; Djajadi, S.; Seth, A.; Hsiang, M.S.; Colford, J.M., Jr.; Reingold, A.; et al. Substantial underestimation of SARS-CoV-2 infection in the United States. *Nat. Commun.* **2020**, *11*, 4507. [CrossRef] [PubMed]
7. Zhu, N.; Zhang, D.; Wang, W.; XingW, L.; Bo, Y.; Jingdong, S.; Xiang, Z.; Baoying, H.; Weifeng, S.; Roujian, L.; et al. A novel coronavirus from patients with pneumonia in China, 2019. *N. Engl. J. Med.* **2020**, *382*, 727–733. [CrossRef]
8. Chen, N.; Zhou, M.; Dong, X.; Qu, J.; Gong, F.; Han, Y.; Qiu, Y.; Wang, J.; Liu, Y.; Wei, Y.; et al. Epidemiological and clinical characteristics of 99 cases of 2019 novel coronavirus pneumonia in Wuhan, China: A descriptive study. *Lancet* **2020**, *395*, 507–513. [CrossRef]
9. Yang, X.; Yu, Y.; Xu, J.; Shu, H.; Xia, J.; Liu, H.; Wu, Y.; Zhang, L.; Yu, Z.; Fang, M.; et al. Clinical course and outcomes of critically ill patients with SARS-CoV-2 pneumonia in Wuhan, China: A single-centred, retrospective, observational study. *Lancet Respir.* **2020**, *8*, 475–481. [CrossRef]
10. WHO. Q&A on Coronaviruses (COVID-19) [EB/OL]. Available online: https://www.who.int/emergencies/diseases/novel-coronavirus-2019/question-and-answers-hub/q-a-detail/q-a-coronaviruses (accessed on 25 January 2021).
11. Chin, A.; Chu, J.L.; Perera, M.; Hui, K.; Yen, H.L.; Chan, M. Stability of SARS-CoV-2 in different environmental conditions. *Lancet Microbe* **2020**, *1*, 1–5. [CrossRef]
12. Stefanou, M.I.; Palaiodimou, L.; Bakola, E.; Smyrnis, N.; Papadopoulou, M.; Paraskevas, G.P.; Rizos, E.; Boutati, E.; Grigoriadis, N.; Krogias, C.; et al. Neurological manifestations of long-COVID syndrome: A narrative review. *Ther. Adv. Chronic Dis.* **2022**, *13*, 20406223221076890. [CrossRef]
13. Centers for Disease Control and Prevention (CDC). Post-COVID Conditions: Information for Healthcare Providers [EB/OL]. Available online: https://www.cdc.gov/coronavirus/2019-ncov/hcp/clinical-care/post-covid-conditions.html (accessed on 3 November 2022).
14. Soriano, J.B.; Murthy, S.; Marshall, J.C.; Relan, P.; Diaz, J.V.; on behalf of the WHO Clinical Case Definition Working Group on Post-COVID-19 Condition. A clinical case definition of post COVID-19 condition by a Delphi consensus. *Lancet Infect. Dis.* **2022**, *22*, e102–e107. [CrossRef]
15. National Institute for Health and Care Excellence. COVID-19 Rapid Guideline: Managing the Long-Term Effects of COVID-19 [M/CD]. NICE. Available online: https://www.nice.org.uk/guidance/ng188/resources/COVID19-rapidguideline-managing-the-longterm-effects-of-COVID19-pdf-51035515742 (accessed on 3 November 2022).
16. Davis, H.E.; Assaf, G.S.; McCorkell, L.; Wei, H.; Low, R.J.; Re'em, Y.; Redfield, S.; Austin, J.P.; Akrami, A. Characterizing long COVID in an international cohort:7 months of symptoms and their impact. *eClinicalMedicine* **2021**, *38*, 101019. [CrossRef]

17. Thompson, E.J.; Williams, D.M.; Walker, A.J.; Mitchell, R.E.; Niedzwiedz, C.L.; Yang, T.C.; Huggins, C.F.; Kwong, A.S.; Silverwood, R.J.; Di Gessa, G.; et al. Long COVID burden and risk factors in 10 UK longitudinal studies and electronic health records. *Nat. Commun.* **2022**, *13*, 3528. [CrossRef] [PubMed]
18. COVID-19 Mental Disorders Collaborators. Global prevalence and burden of depressive and anxiety disorders in 204 countries and territories in 2020 due to the COVID-19 pandemic. *Lancet* **2021**, *398*, 1700–1712. [CrossRef] [PubMed]
19. Montefusco, L.; Ben Nasr, M.; D'Addio, F.; Loretelli, C.; Rossi, A.; Pastore, I.; Daniele, G.; Abdelsalam, A.; Maestroni, A.; Dell'Acqua, M.; et al. Acute and long-term disruption of glycometabolic control after SARS-CoV-2 infection. *Nat. Metab.* **2021**, *3*, 774–785. [CrossRef] [PubMed]
20. Mehandru, S.; Merad, M. Pathological sequelae of long-haul COVID. *Nat. Immunol.* **2022**, *23*, 194–202. [CrossRef] [PubMed]
21. Bowe, B.; Xie, Y.; Xu, E.; Al-Aly, Z. Kidney outcomes in long COVID. *J. Am. Soc. Nephrol.* **2021**, *32*, 2851–2862. [CrossRef]
22. Weng, J.; Li, Y.; Li, J.; Shen, L.; Zhu, L.; Liang, Y.; Lin, X.; Jiao, N.; Cheng, S.; Huang, Y.; et al. Gastrointestinal sequelae 90 days after discharge for COVID-19. *Lancet Gastroenterol. Hepatol.* **2021**, *6*, 344–346. [CrossRef]
23. Freeman, E.E.; McMahon, D.E.; Lipoff, J.B.; Rosenbach, M.; Kovarik, C.; Desai, S.R.; Harp, J.; Takeshita, J.; French, L.E.; Lim, H.W.; et al. The spectrum of COVID-19-associated dermatologic manifestations: An international registry of 716 patients from 31 countries. *J. Am. Acad. Dermatol.* **2020**, *83*, 1118–1129. [CrossRef] [PubMed]
24. Sanyaolu, A.; Marinkovic, A.; Prakash, S.; Zhao, A.; Balendra, V.; Haider, N.; Jain, I.; Simic, T.; Okorie, C. Post-acute sequelae in COVID-19 survivors: An overview. *SN Compr. Clin. Med.* **2022**, *4*, 91. [CrossRef]
25. Truffaut, L.; Demey, L.; Bruyneel, A.V.; Roman, A.; Alard, S.; de Vos, N.; Bruyneel, M. Post-discharge critical COVID-19 lung function related to severity of radiologic lung involvement at admission. *Respir. Res.* **2021**, *22*, 29. [CrossRef]
26. Kleinstreuer, C.; Zhang, Z.; Donohue, J.F. Targeted drug-aerosol delivery in the human respiratory system. *Annu. Rev. Biomed. Eng.* **2008**, *10*, 195–220. [CrossRef]
27. Respiration in Human Beings. Available online: http://www.tutorvista.com/biology/respiration-in-human-beings (accessed on 12 January 2023).
28. Lintermann, A.; Schröder, W. Simulation of aerosol particle deposition in the upper human tracheobronchial tract. *Eur. J. Mech. -B/Fluids* **2017**, *63*, 73–89. [CrossRef]
29. Zhang, T.; Gao, B.; Zhou, Z.; Chang, Y. The movement and deposition of PM 2.5 in the upper respiratory tract for the patients with heart failure: An elementary CFD study. *Biomed. Eng. Online* **2016**, *15*, 138. [CrossRef] [PubMed]
30. Djojodihardjo, H.; Ahmed, R.I. CFD simulation of Coandfi effect on the upper respiratory system. *J. Med. Imaging Health Inf.* **2016**, *6*, 1526–1535.
31. Anderson, H.R.; Atkinson, R.W.; Peacock, J.L.; Marston, L.; Konstantinou, K. *; World Health Organization. Meta-Analysis of Time Series Studies and Panel Studies of Particulate Matter (PM) and Ozone*; WHO Regional Office for Europe: København, Denmark, 2004; pp. 1–73.
32. Oberdorster, G.; Utell, M.J. Ultrafine particles in the urban air: To the respiratory tract-and beyond? *Environ. Health Perspect.* **2002**, *110*, 440–441. [CrossRef]
33. Brunekreef, B. Air pollution and life expectancy: Is there a relation? *Occup. Environ. Med.* **1997**, *54*, 781–784. [CrossRef]
34. Pope Iii, C.A.; Burnett, R.T.; Thun, M.J.; Calle, E.E.; Krewski, D.; Ito, K.; Thurston, G.D. Lung cancer, cardiopulmonary mortality, and long-term exposure to fine particulate air pollution. *J. Am. Med. Assoc.* **2002**, *287*, 1132–1141. [CrossRef]
35. Rogers, J.F.; Dunlop, A.L. Air pollution andvery low birth weight infants: A target population. *Pediatrics* **2006**, *118*, 156–164. [CrossRef]
36. Samet, J.M.; Dominici, F.; Curriero, F.C.; Coursac, M.S.; Scott, L.Z. Fine particulate air pollution and mortality in 20 U.S. cities, 1987–1994. *N. Engl. J. Med.* **2000**, *343*, 1742–1749. [CrossRef]
37. Jungblut, D.; Queisser, G.; Wittum, G. Inertia based filtering of high resolution images using a gpu cluster. *Comput. Vis. Sci.* **2012**, *14*, 181–186. [CrossRef]
38. Tsai, S.S.; Chang, C.C.; Yang, C.Y. Fine particulate air pollution and hospital admissions for chronic obstructive pulmonary disease: A case-crossover study in Taipei. *Int. J. Environ. Res. Public Health* **2013**, *10*, 6015–6026. [CrossRef]
39. Tian, Y.; Xiang, X.; Juan, J.; Sun, K.; Song, J.; Cao, Y.; Hu, Y. Fine particulate air pollution and hospital visits for asthma in Beijing, China. *Environ. Pollut.* **2017**, *230*, 227–233. [CrossRef] [PubMed]
40. Turner, M.C.; Krewski, D.; Pope Iii, C.A.; Chen, Y.; Gapstur, S.M.; Thun, M.J. Long-term ambient fine particulate matter air pollution and lung cancer in a large cohort of never-smokers. *Am. J. Respir. Crit. Care Med.* **2011**, *184*, 1374–1381. [CrossRef] [PubMed]
41. Dockery, D.W.; Pope, C.A.; Xu, X.; James, H.W.; Martha, E.F.; Benjamin, G.F.; Frank, E.S. An association between air pollution and mortality in six U. S. cities. *N. Engl. J. Med.* **1993**, *329*, 1753–1759. [CrossRef] [PubMed]
42. Baur, X.; Sanyal, S.; Abraham, J.L. Mixed-dust pneumoconiosis: Review of diagnostic and classification problems with presentation of a work-related case. *Sci. Total Environ.* **2019**, *652*, 413–421. [CrossRef] [PubMed]
43. Mandrioli, D.; Schlünssen, V.; Adam, B.; Cohen, R.A.; Colosio, C.; Chen, W.; Fischer, A.; Godderis, L.; Goen, T.; Ivanov, I.D.; et al. WHO/ILO work-related burden of disease and injury: Protocol for systematic reviews of occupational exposure to dusts and/or fibres and of the effect of occupational exposure to dusts and/or fibres on pneumoconiosis. *Environ. Int.* **2018**, *119*, 174–185. [CrossRef]
44. Guo Xinbiao; Wei Hongying. Research progress on health effects of atmospheric PM2.5. *Sci. Bull.* **2013**, *58*, 1171–1177.

45. The epidemiological characteristics of an outbreak of 2019 novel coronavirus diseases (COVID-19) in China. *Zhonghua Liu Xing Bing Xue Za Zhi* **2020**, *41*, 145–151. [CrossRef]
46. Luo, J.; Rizvi, H.; Egger, J.V.; Preeshagul, I.R.; Wolchok, J.D.; Hellmann, M.D. Impact of PD-1 Blockade on Severity of COVID-19 in Patients with Lung Cancers. *Cancer Discov.* **2020**, *10*, 1121–1128. [CrossRef]
47. Liu, Y.; Kan, H.; Xu, J.; Rogers, D.; Li, P.; Ye, X.; Chen, R.; Zhang, Y.; Wang, W. Temporal relationship between hospital admissions for pneumonia and weather conditions in Shanghai, China: A time-series analysis. *BMJ Open* **2014**, *4*, e004961. [CrossRef]
48. Barreca, A.I. Climate change, humidity, and mortality in the United States. *J. Environ. Econ. Manag.* **2012**, *63*, 19–34. [CrossRef]
49. Tao, Y.; Song, J.; Qiang, L.; Wang, Y.; Li, Z. Time series research on meteorological factors and measles incidence in Chengguan District of Lanzhou City. *Chin. Environ. Sci.* **2014**, *34*, 2964–2969.
50. Jaakkola, K.; Saukkoriipi, A.; Jokelainen, J.; Juvonen, R.; Kauppila, J.; Vainio, O.; Ziegler, T.; Ronkko, E.; Jaakkola, J.; Ikaheimo, T. Decline in temperature and humidity increases the occurrence of influenza in cold climate. *Environ. Health* **2014**, *13*, 22. [CrossRef] [PubMed]
51. Chung, J.Y.; Honda, Y.; Hong, Y.C.; Pan, X.C.; Guo, Y.L.; Kim, H. Ambient temperature and mortality: An international study in four capital cities of East Asia. *Sci. Total Environ.* **2009**, *408*, 390–396. [CrossRef] [PubMed]
52. Bahmanzadeh, H.; Abouali, O.; Faramarzi, M.; Ahmadi, G. Numericalsimulation of airflow and micro-particle deposition in human nasalairway pre-and post-virtual sphenoidotomy surgery. *Comput. Biol. Med.* **2015**, *61*, 8–18. [CrossRef]
53. Wang, S.; Gu, X.; Xu, S. Research progress in numerical simulation of physical field and gas-solid two-phase flow in the nasal cavity. *Int. J. Otorhinolaryngol.-Head Neck Surg.* **2016**, *40*, 65–70.
54. Su, Y.; Liu, Y.; Sun, X. Numerical simulation study of nasal airflow field in healthy Chinese. *Chin. Dep. Otorhinolaryngol. Head Neck Surg.* **2015**, *562*, 545–547.
55. Cui, X.; Gutheil, E.; Baumann, I. CFD Study of the Flow Field and Particle Dispersion and Deposition in the Upper Human Respiratory System. Ph.D. Thesis, Ruperto-Carola University of Heidelberg, Heidelberg, Germany, 2012.
56. Jeong, S.J.; Kim, W.S.; Sung, S.J. Numerical investigation on the flow characteristics and aerodynamic force of the upper airway of patient with obstructive sleep apnea using computational fluid dynamics. *Med. Eng. Phys.* **2007**, *29*, 637–651. [CrossRef]
57. Wang, Y.; Wang, J.; Liu, Y.; Yu, S.; Sun, X.; Li, S.; Shen, S.; Zhao, W. Fluid-structure interaction modeling of upper airways before and after nasal surgery for obstructive sleep apnea. *Int. J. Numer. Method Biomed Eng.* **2012**, *28*, 528–546. [CrossRef]
58. Cisonni, J.; Lucey, A.D.; King, A.J.; Islam, S.M.S.; Lewis, R.; Mithran, G. Numerical simulation of pharyngeal airflow applied to obstructive sleep apnea: Effect of the nasal cavity in anatomically accurate airway models. *Med. Biol. Eng. Comput.* **2015**, *53*, 1129–1139. [CrossRef]
59. Cheng, Y.S.; Zhou, Y.; Chen, B.T. Particle deposition in a cast of human oral airways. *Aerosol Sci. Technol.* **1999**, *31*, 286–300. [CrossRef]
60. Grgic, B.; Finlay, W.H.; Heenan, A.F. Regional aerosol deposition and flow measurements in an idealized mouth and throat. *J. Aerosol Sci.* **2004**, *35*, 21–32. [CrossRef]
61. Martonen, T.; Zhang, Z.; Lessmann, R.C. Fluid Dynamics of the Human Larynx and Upper TB Airways. *Aerosol Sci. Technol.* **1993**, *19*, 133–156. [CrossRef]
62. Xi, J.; Yuan, J.E.; Yang, M.; Si, X.; Zhou, Y.; Cheng, Y.S. Parametric study on mouth-throat geometrical factors on deposition of orally inhaled aerosols. *J. Aerosol Sci.* **2016**, *99*, 94–106. [CrossRef]
63. Grgic, B.; Martin, A.R.; Finlay, W.H. The effect of unsteady flow rate increase on in vitro mouth–throat deposition of inhaled boluses. *J. Aerosol Sci.* **2006**, *37*, 1222–1233. [CrossRef]
64. Kim, C.S.; Fisher, D.M. Deposition characteristics of aerosol particles in sequentially bifurcating airway models. *Aerosol Sci. Technol.* **1999**, *31*, 198–220. [CrossRef]
65. Zhou, Y.; Cheng, Y.S. Particle deposition in a cast of human tracheobronchial airways. *Aerosol Sci. Technol.* **2005**, *39*, 492–500. [CrossRef]
66. Li, F.S.; Xu, X.X.; Sun, D.; Zhao, X.G.; Yang, M.; Tan, S.L. Experimental study on deposition of aerosol particles in human upper respiratory tract model. *Med. Biomech.* **2013**, *56*, 135–141.
67. Phuong, N.L.; Ito, K. Investigation of flow pattern in upper human airway including oral and nasal inhalation by PIV and CFD. *Build. Environ.* **2015**, *94*, 504–515. [CrossRef]
68. Jia, L.; Zhang, L.; Yu, S. Deposition of non-spherical microparticles in the human upper respiratory tract. *Particuology* **2018**, *36*, 185–189. [CrossRef]
69. Kiasadegh, M.; Emdad, H.; Ahmadi, G.; Abouali, O. Transient numerical simulation of airflow and fibrous particles in a human upper airway model. *J. Aerosol Sci.* **2020**, *140*, 105480. [CrossRef]
70. Huang, J.; Zhang, L. Numerical simulation of micro-particle deposition in a realistic human upper respiratory tract model during transient breathing cycle. *Particuology* **2011**, *9*, 424–431. [CrossRef]
71. Chen, X.; Kleinstreuer, C.; Zhong, W.; Zhou, X. Effects of thermal airflow and mucus-layer interaction on hygroscopic droplet deposition in a simple mouth–throat model. *Aerosol Sci. Technol.* **2018**, *52*, 900–912. [CrossRef]
72. Taherian, S.; Rahai, H.; Gomez, B.Z.; Waddington, T. Particulates depositions in patient-specific simulations of respiratory system. In Proceedings of the ASME 2014 International Mechanical Engineering Congress and Exposition, Montreal, QC, Canada, 14–20 November 2014; Volume 3.

73. Van Rhein, T.; Alzahrany, M.; Banerjee, A.; Salzman, G. Fluid flow and particle transport in mechanically ventilated airways. Part I. Fluid flow structures. *Med. Biol. Eng. Comput.* **2016**, *54*, 1085–1096. [CrossRef] [PubMed]
74. Sracic, M.K. Modeled regional airway deposition of inhaled particles in athletes at exeron. *J. Aerosol Sci.* **2016**, *99*, 54–63. [CrossRef]
75. Islam, M.S.; Saha, S.C.; Sauret, E.; Gu, Y.T. Effects of velocity on diesel exhaust particle transpot tiand deposition in the central airways of the human lung. *ACCM* **2015**, *18*, 175–187.
76. Rahimi-Gorji, M.; Pourmehran, O.; Gorji-Bandpy, M.; Gorji, T.B. CFD simulation of airflow behavior and particle transport and deposition in different breathing conditions through the realistic model of human airways. *J. Mol. Liq.* **2015**, *209*, 121–133. [CrossRef]
77. Yu, S.; Wang, J.; Sun, X. Numerical Simulation of Particle Deposition in the Respiratory Tract. *Med. Biomech.* **2016**, *31*, 193–198.
78. Dastan, A.; Abouali, O.; Ahmadi, G. CFD simulation of total and regional fiber deposition in human nasal cavities. *J. Aerosol Sci.* **2014**, *69*, 132–149. [CrossRef]
79. Sturm, R. Bioaerosols in the lungs of subjects with different ages-part 1: Deposition modeling. *J. Transl. Med.* **2016**, *4*, 211. [CrossRef]
80. Kleinstreuer, C.; Zhang, Z.; Kim, C.S. Combined inertial and gravitational deposition of microparticles in small model airways of a human respiratory system. *J. Aerosol Sci.* **2007**, *38*, 1047–1061. [CrossRef]
81. Nicolaou, L. Inertial and gravitational effects on aerosol deposition in the conducting airways. *J. Aerosol Sci.* **2018**, *120*, 32–51. [CrossRef]
82. Tian, L.; Ahmadi, G. Transport and deposition of nano-fibers in human upper tracheobronchial airways. *J. Aerosol Sci.* **2016**, *91*, 22–32. [CrossRef]
83. Feng, Y.; Kleinstreuer, C.; Rostami, A. Evaporation and condensation of multicomponent electronic cigarette droplets and conventional cigarette smoke particles in an idealized G3–G6 triple bifurcating unit. *J. Aerosol Sci.* **2015**, *80*, 58–74. [CrossRef]
84. Chen, X.; Zhong, W.; Zhou, X.; Jin, B.; Sun, B. CFD–DEM simulation of particle transport and deposition in pulmonary airway. *Powder Technol.* **2012**, *228*, 309–318. [CrossRef]
85. Deng, Q.; Ou, C.; Shen, Y.M.; Xiang, Y.; Miao, Y.; Li, Y. Health effects of physical activity as predicted by particle deposition in the human respiratory tract. *Sci. Total Environ.* **2019**, *657*, 819–826. [CrossRef]
86. Li, R.; Zhao, X.; Liu, Y. Numerical simulation and experimental research progress of inhalable particulate matter deposition in the human respiratory system. *J. Biomed. Eng.* **2017**, *34*, 637–642.
87. Kabilan, S.; Suffield, S.R.; Recknagle, K.P.; Jacob, R.E.; Einstein, D.R.; Kuprat, A.P.; Carson, J.P.; Colly, S.M.; Saunders, J.H.; Hines, S.A.; et al. Computational fluid dynamics modeling of Bacillus anthracis spore deposition in rabbit and human respiratory airways. *J. Aerosol Sci.* **2016**, *99*, 64–77. [CrossRef]
88. Islam, M.S.; Saha, S.C.; Sauret, E.; Gu, Y.T. Numerical investigation of diesel exhaust particle transport and deposition in up to 17 generations of the lung airway. In Proceedings of the 20th Australasian Fluid Mechanics Conference 2016, Perth, Australia, 5–8 December 2016.
89. Available online: https://baike.baidu.com/item/%E8%82%BA%E8%85%BA%E6%B3%A1/10975738 (accessed on 10 January 2023).
90. Moskal, A. Modeling of he influence of tissue mechanical properties on the process of aerosol particles deposition in a model of human alveolus. *J. Drug Deliv. Sci. Technol.* **2012**, *22*, 153–159.
91. Darquenne, C.; Harrington, L.; Prisk, G.K. Alveolar duct expansion greatly enhances aerosol deposition: A three-dimensional computational fluid dynamics study. *Philos Trans. A Math Phys. Eng. Sci.* **2009**, *367*, 2333–2346. [CrossRef]
92. Sznitman, J.; Heimsch, F.; Heimsch, T.; Rusch, D.; Rösgen, T. Three-dimensional convective alveolar flow induced by rhythmic breathing motion of the pulmonary acinus. *J. Biomech. Eng.* **2007**, *129*, 658–665. [CrossRef]
93. Sznitman, J.; Heimsch, T.; Wildhaber, J.H.; Tsuda, A.; Rösgen, T. Respiratory flow phenomena and gravitational deposition in a three-dimensional space-filling model of the pulmonary acinar tree. *J. Biomech. Eng.* **2009**, *131*, 031010. [CrossRef] [PubMed]
94. Haber, S.; Yitzhak, D.; Tsuda, A. Gravitational deposition in a rhythmically expanding and contracting alveolus. *Natl. Libr. Medcine* **2003**, *95*, 657–671. [CrossRef] [PubMed]
95. Ching, J.; Kajino, M. Aerosol mixing state matters for particles deposition in human respiratory system. *Sci. Rep.* **2018**, *8*, 8864. [CrossRef] [PubMed]
96. Darquenne, C. Deposition Mechanisms. *J. Aerosol Med. Pulm. Drug Deliv.* **2020**, *33*, 181–185. [CrossRef]
97. Deng, Q.; Deng, L.; Miao, Y.; Guo, X.; Li, Y. Particle deposition in the human lung: Health implications of particulate matter from different sources. *Environ. Res.* **2019**, *169*, 237–245. [CrossRef]
98. Manojkumar, N.; Srimuruganandam, B.; Nagendra, S.S. Application of multiple-path particle dosimetry model for quantifying age specified deposition of particulate matter in human airway. *Ecotoxicol. Environ. Saf.* **2019**, *168*, 241–248. [CrossRef]
99. Manojkumar, N.; Srimuruganandam, B. Age-specific and seasonal deposition of outdoor and indoor particulate matter in human respiratory tract. *Atmos. Pollut. Res.* **2022**, *13*, 101298. [CrossRef]
100. Khan, S.; Gurjar, B.R.; Sahu, V. Deposition modeling of ambient particulate matter in the human respiratory tract. *Atmos. Pollut. Res.* **2022**, *13*, 101565. [CrossRef]
101. Liu, M.; Guo, W.; Zhao, L.; Yang, H.; Fang, Q.; Li, M.; Shu, J.; Chen, S.; Lai, X.; Yang, L.; et al. Association of personal fine particulate matter and its respiratory tract depositions with blood pressure in children: From two panel studies. *J. Hazard. Mater.* **2021**, *416*, 126120. [CrossRef]

102. Zoladz, J.A.; Nieckarz, Z. Marathon race performance increases the amount of particulate matter deposited in the respiratory system of runners: An incentive for "clean air marathon runs". *PeerJ* **2021**, *9*, e11562. [CrossRef]
103. Khajeh-Hosseini-Dalasm, N.; Longest, P.W. Deposition of particles in the alveolar airways: Inhalation and Breath-Hold with pharmaceutical aerosols. *J. Aerosol Sci.* **2015**, *79*, 15–30. [CrossRef]
104. Kolanjiyil, A.V.; Kleinstreuer, C. Modeling Airflow and Particle Deposition in a Human Acinar Region. *Comput. Math. Methods Med.* **2019**, *2019*, 5952941. [CrossRef] [PubMed]
105. Schittny, J.C.; Mund, S.I.; Stampanoni, M. Evidence and structural mechanism for late lung alveolarization. *Am. J. Physiol. Lung Cell. Mol. Physiol.* **2008**, *294*, L246–L254. [CrossRef] [PubMed]
106. Moraes, C.; Mehta, G.; Lesher-Perez, S.C.; Takayama, S. Organs-on-a-chip: A focus on compartmentalized microdevices. *Ann. Biomed. Eng.* **2012**, *40*, 1211–1227. [CrossRef] [PubMed]
107. Muneswarao, J.; Verma, A.K.; Hassali, M.A.A. Global initiative for chronic obstructive lung disease (GOLD) 2018 report: Highlighting an incorrect information. *Pulm. Pharmacol. Ther.* **2018**, *49*, 10. [CrossRef]
108. Zhang, S.; Zhang, M.; Feng, G. PCDD/Fs pollution in the workshop of automobile foundry and assessment of respiratory exposure of workshop workers. *China Environ. Sci.* **2015**, *35*, 3779–3785.
109. Samarghandi, A.; Ioachimescu, O.C.; Qayyum, R. Association between peak inspiratory flow rate and hand grip muscle strength in hospitalized patients with acute exacerbation of chronic obstructive pulmonary disease. *PLoS ONE* **2020**, *15*, e0227737. [CrossRef]
110. Darquenne, C.; Lamm, W.J.; Fine, J.M.; Corlet, R.A.; Gelenny, R. Total and regional deposition of inhaled aerosols in supine healthy subjects and subjects with mild-to-moderate COPD. *J. Aerosol Sci.* **2016**, *99*, 27–39. [CrossRef]
111. Ganguly, K.; Carlander, U.; Garessus, E.D.; Fridén, M.; Eriksson, U.G.; Tehler, U.; Johanson, G. Computational modeling of lung deposition of inhaled particles in chronic obstructive pulmonary disease (COPD) patients: Identification of gaps in knowledge and data. *Crit. Rev. Toxicol.* **2019**, *49*, 160–173. [CrossRef]
112. Wang, Y.B.; Watts, A.B.; Peters, J.I.; Williams, R.O. The impact of pulmonary diseases on the fate of inhaled medicines—A review. *Int. J. Pharm.* **2014**, *461*, 112–128. [CrossRef]
113. Zhuang Jiawei; Diao Yongfa; Chu Minghao; Shen Henggen. Movement and deposition characteristics of inhalable particulate matter in different obstructive airways. *Chin. Environ. Sci.* **2021**, *41*, 3349–3359.
114. Tohidi, R.; Sajadi, B.; Ahmadi, G. The effect of nasal airway obstruction on the dispersion and deposition of inhaled volatile droplets in the human nasal cavity: A numerical study. *J. Aerosol Sci.* **2020**, *150*, 105650. [CrossRef]
115. Zhang, W.; Xiang, Y.; Lu, C.; Deng, Q. Numerical modeling of particle deposition in the conducting airways of asthmatic children. *Med. Eng. Phys.* **2020**, *76*, 40–46. [CrossRef] [PubMed]
116. Luo, H.Y.; Liu, Y.; Yang, X.L. Particle deposition in obstructed airways. *J. Biomech.* **2007**, *40*, 3096–3104. [CrossRef]
117. Prinz, A.L.; Richter, D.J. Long-term exposure to fine particulate matter air pollution: An ecological study of its effect on COVID-19 cases and fatality in Germany. *Environ. Res.* **2022**, *204*, 111948. [CrossRef]
118. Bianconi, V.; Bronzo, P.; Banach, M.; Sahebkar, A.; Mannarino, M.; Pirro, M. Particulate matter pollution and the COVID-19 outbreak: Results from Italian regions and provinces. *Arch. Med. Sci.* **2020**, *16*, 985–992. [CrossRef]
119. Mehmood, K.; Iqbal, M.; Abrar, M.M. Can exposure to PM2.5 particles increase the incidence of coronavirus disease 2019 (COVID-19)? *Sci. Total Environ.* **2020**, *741*, 140441. [CrossRef]
120. Abrar, M.M.; Iqbal, M.; Haider, E.; Shoukat, H.M.H. Can PM2.5 pollution worsen the death rate due to COVID-19 in India and Pakistan? *Sci. Total Environ.* **2020**, *742*, 140557.
121. Renard, J.B.; Surcin, J.; Annesi-Maesano, I.; Delaunay, G.; Poincelet, E.; Dixsaut, G. Relation between PM2.5 pollution and COVID-19 mortality in Western Europe for the 2020–2022 period. *Sci. Total Environ.* **2022**, *848*, 157579. [CrossRef]
122. Rodríguez-Urrego, D.; Rodríguez-Urrego, L. Air quality during the COVID-19: PM2.5 analysis in the 50 most polluted capital cities in the world. *Environ. Pollut.* **2020**, *266*, 115042. [CrossRef]
123. Mathew, T.; Madhavi, N. Air Quality During COVID-19: Analysis of Particulate Matter for a Coastal Urban Station Visakhapatnam (India). *Lett. Appl. Nano Biosci.* **2020**, *10*, 1925–1935.
124. Cruz, R.; Lima-Silva, A.E.; Bertuzzi, R.; Hoinaski, L. Exercising under particulate matter exposure: Providing theoretical support for lung deposition and its relationship with COVID-19. *Environ. Res.* **2021**, *202*, 111755. [CrossRef] [PubMed]
125. Workman, A.D.; Jafari, A.; Xiao, R.; Bleier, B.S. Airborne aerosol olfactory deposition contributes to anosmia in COVID-19. *PLoS ONE* **2021**, *16*, e0244127. [CrossRef] [PubMed]
126. Davis, M.E.; Chen, Z.; Dong, M.S. Nanoparticle therapeutics:an emerging treatment modality for cancer. *Nat. Rev. Drug Discov.* **2008**, *7*, 771–782. [CrossRef]
127. Kreuter, J. Nanoparticulate systems for brain delivery of drugs. *Adv. Drug Deliv. Rev.* **2001**, *47*, 65–81. [CrossRef]
128. Broday, D. Deposition of ultrafine particles at carinal ridges of the upper bronchial airways. *Aerosol Sci. Technol.* **2004**, *38*, 991–1000. [CrossRef]

129. Isaacs, K.K.; Martonen, T.B. Particle deposition in children's lungs: Theory and experiment. *J. Aerosol Med.* **2005**, *18*, 337–353. [CrossRef]
130. Feng, Y.; Xu, Z.; Haghnegahdar, A. Computational Fluid·Particle Dynamics Modeling for Unconventional Inhaled Aerosols in Human Respiratory Systems. *Aerosols Sci. Case Stud.* **2016**, *35*, 49–84.